AD-A066 094 SRI INTERNATIONAL MENLO PARK CA F/G 20/14
COMPARATIVE EQUATORIAL SCINTILLATION MORPHOLOGY--AMERICAN AND P--ETC(U)
JUN 78 R C LIVINGSTON DNA001-77-C-0220
UNCLASSIFIED DNA-4644T NL

1 OF 1
ADA
066094

END
DATE
FILMED
5 79
DDC

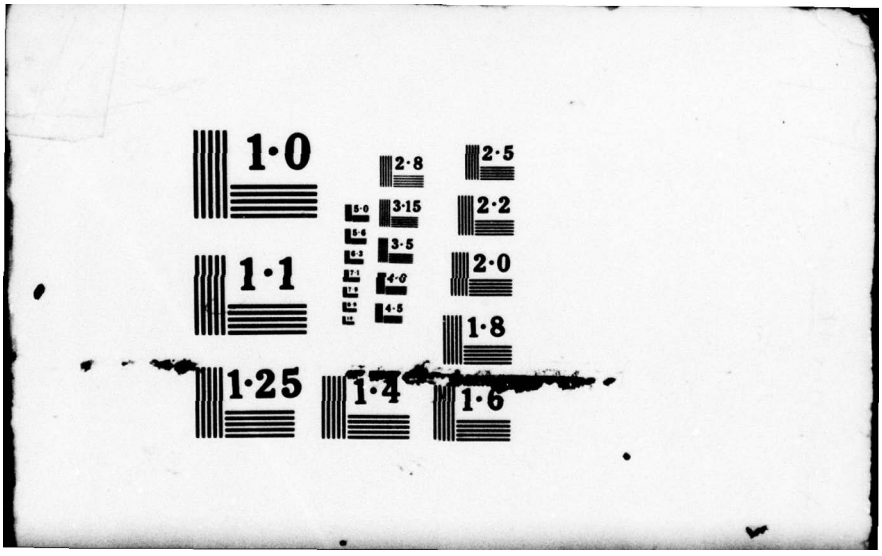
1·0
1·1
1·25
1·4
1·6
1·8
2·0
2·2
2·5
2·8
3·15
3·5
4·0
4·5
5·0

(12) NW LEVEL III

DNA 4644T



# COMPARATIVE EQUATORIAL SCINTILLATION MORPHOLOGY -- AMERICAN AND PACIFIC SECTORS

Robert C. Livingston

SRI International
333 Ravenswood Avenue
Menlo Park, California 94025

30 June 1978

Topical Report 3 for Period 1 June 1977—30 June 1978

CONTRACT No. DNA 001-77-C-0220



APPROVED FOR PUBLIC RELEASE;
DISTRIBUTION UNLIMITED.

THIS WORK SPONSORED BY THE DEFENSE NUCLEAR AGENCY
UNDER RDT&E RMSS CODE B322078462 I25AAXHX63340 H2590D.

Prepared for
Director
DEFENSE NUCLEAR AGENCY
Washington, D. C. 20305

Destroy this report when it is no longer needed. Do not return to sender.

PLEASE NOTIFY THE DEFENSE NUCLEAR AGENCY, ATTN: TISI, WASHINGTON, D.C. 20305, IF YOUR ADDRESS IS INCORRECT, IF YOU WISH TO BE DELETED FROM THE DISTRIBUTION LIST, OR IF THE ADDRESSEE IS NO LONGER EMPLOYED BY YOUR ORGANIZATION.

UNCLASSIFIED

SECURITY CLASSIFICATION OF THIS PAGE (When Data Entered)

## REPORT DOCUMENTATION PAGE

READ INSTRUCTIONS BEFORE COMPLETING FORM

1. REPORT NUMBER: DNA 4644T

2. GOVT ACCESSION NO.

3. RECIPIENT'S CATALOG NUMBER

4. TITLE (and Subtitle): COMPARATIVE EQUATORIAL SCINTILLATION MORPHOLOGY--AMERICAN AND PACIFIC SECTORS.

5. TYPE OF REPORT & PERIOD COVERED: Topical Report, Period 1 Jun 77 — 30 Jun 78

6. PERFORMING ORG. REPORT NUMBER: SRI Project 6434

7. AUTHOR(s): Robert C. Livingston

8. CONTRACT OR GRANT NUMBER(s): DNA 001-77-C-0220

9. PERFORMING ORGANIZATION NAME AND ADDRESS:
SRI International
333 Ravenswood Avenue
Menlo Park, California 94025

10. PROGRAM ELEMENT, PROJECT, TASK AREA & WORK UNIT NUMBERS: Subtask I25AAXHX633-40

11. CONTROLLING OFFICE NAME AND ADDRESS:
Director
Defense Nuclear Agency
Washington, D.C. 20305

12. REPORT DATE: 30 June 1978

13. NUMBER OF PAGES: 54

14. MONITORING AGENCY NAME & ADDRESS (if different from Controlling Office): 6710H

15. SECURITY CLASS (of this report): UNCLASSIFIED

15a. DECLASSIFICATION/DOWNGRADING SCHEDULE

16. DISTRIBUTION STATEMENT (of this Report)

Approved for public release; distribution unlimited.

17. DISTRIBUTION STATEMENT (of the abstract entered in Block 20, if different from Report)

18. DNA, SBIE

19. 4644T, AD-E300469

18. SUPPLEMENTARY NOTES

This work sponsored by the Defense Nuclear Agency under RDT&E RMSS Code B322078462 I25AAXHX63340 H2590D.

19. KEY WORDS (Continue on reverse side if necessary and identify by block number)

Amplitude Scintillation
Satellite Propagation
Equatorial Ionosphere

20. ABSTRACT (Continue on reverse side if necessary and identify by block number)

This report examines the severity of radio-wave amplitude scintillation measured at two stations near the equator, but far apart in longitude: Kwajalein Atoll in the Marshall Islands, and Ancon, Peru. The data used are observations of the Wideband satellite signal intensity at VHF, UHF, and L-band frequencies. These are presented in terms of the cumulative distribution of $S_4$ index, which provides a precise measure of the level of disturbance that can be readily related to the distribution of signal intensity.

DD FORM 1 JAN 73 1473 EDITION OF 1 NOV 65 IS OBSOLETE

UNCLASSIFIED

SECURITY CLASSIFICATION OF THIS PAGE (When Data Entered)

410281

JCB

20. ABSTRACT (Continued)

The seasonal behavior of the scintillation at the two stations is similar, with each showing a broad 8-to-9-month disturbed season centered about local summer. There is little difference in the occurrence or severity of gigahertz scintillation at the two stations. However, there is a systematic difference between the frequency dependences of the scintillation.

The latitude distributions of scintillation show the expected enhancement from propagation geometry at low elevation angles. When these effects are removed to obtain irregularity source strength, the irregularity source regions are found at some distance from the magnetic equator.

It is suggested that the weak-to-moderate scintillation that dominates the observations arises from interactions between neutral waves and ionization in the F region.

## EXECUTIVE SUMMARY

Ionospheric scintillation has been, and remains, a problem for a variety of satellite communication/navigation systems operating near the equator. Accordingly, there has been a series of scintillation experiments over the past two decades designed to study various aspects of the problem. The Wideband satellite allows us to expand the scope of these previous studies by virtue of two equatorial observing stations, one in the central Pacific and one in South America, and because of its multifrequencies, which range from VHF to S-band.

In this report we study and compare the seasonal and latitudinal variations in intensity scintillation severity at the two equatorial stations. Our purpose is twofold--first, to provide the system designer with adequate multifrequency intensity statistics, and second, to learn something about the long-term temporal and spatial conditions under which the scintillation-producing irregularities develop.

The first purpose is satisfied by our accumulated scintillation index statistics, which are in a format readily converted to system fade margin requirements as a function of frequency, season, and latitude.

As for the second purpose, which relates to the physics of the irregularity mechanisms, our primary findings are as follows:

- Rather than equinoctial peaks in the scintillation as some previous experimentors have described, we see a broad, structured 8-to-9-month scintillation season centered on local summer at both stations.
- There is little difference between the occurrence or severity of gigahertz scintillation at Kwajalein and Ancon, as has recently been suggested. However, a slight difference in irregularity spectral slope causes a difference in the frequency

dependence of scintillation between the two stations. As a result, the scintillation at the lower frequencies is more severe at Ancon.

- By removing, by way of modeling, geometrical propagation effects from the latitudinal distributions of scintillation, we find irregularity source regions removed from the magnetic dip equator. The width and location of these regions, which are different at Ancon and Kwajalein, change with season.

Our interpretation of these results and other features in the data is that there are multiple mechanisms producing equatorial scintillation irregularities. For the weaker scatter observed at VHF we are probably dealing with neutral-wave perturbation-generated irregularities. At L-band, the scintillation is produced by orders-of-magnitude-stronger, yet less prevalent irregularities, which are most likely a product of the Rayleigh-Taylor instability.

CONTENTS

## ILLUSTRATIONS

# I INTRODUCTION

For decades the equatorial ionosphere has been known to be a region in which major electron density irregularities routinely occur. The kilometer-to-tens of kilometers portion of the irregularity scale size continuum produces a distinct ionosonde signature that has been observed for many years; hence, the name equatorial spread-F. With the advent of communication/navigation satellites, another aspect of equatorial irregularities has become important. Smaller-scale structures, in the tens-of-meters-to-kilometer regime, cause fading or scintillation of radio-wave signals propagating through the ionosphere. At UHF frequencies, the signals are often disturbed beyond usefulness, and even at gigahertz frequencies communications are occasionally degraded.

Having been initially motivated by these practical aspects of satellite communications, the physics of equatorial irregularity development is now being vigorously pursued. The bulk of the current experimental data has come from in-situ satellites (e.g., McClure et al., 1977) and rocket probes (e.g., Kelley et al., 1976; Morse et al., 1977) for medium-to-large-scale irregularities, and from radar backscatter (Woodman and La Hoz, 1976; Tsunoda et al., 1978) for meter-size and smaller structures. What is emerging is a consistent picture of irregularity development. Large, isolated regions of irregularity structure are observed with density variations of the order of magnitude of the background ionization, often associated with a large-scale ionization depletion. In some cases, the radar data indicate irregularities extending vertically well through the F-layer peak. An attractive theory to explain such structures is the Rayleigh-Taylor mechanism, in which a large (about 100 km) volume of depleted ionization is driven through the F-region by a gravitational instability (Scannapieco and Ossakow, 1976). The depleted volume leaves a trail, or plume, of small-scale (tens of centimeters to a meter) irregularities surrounding the depletion, which itself is unstable to a gradient-drift type mechanism. This mechanism is believed to produce the

intense irregularities that cause equatorial gigahertz scintillation. A second, and perhaps complementary, irregularity development mechanism is spatial resonance (Rottger, 1977), in which a neutral wave traveling with a phase velocity equal to the local plasma velocity becomes amplified. Eventually the amplified TID nonlinearly steepens, producing smaller-scale irregularities. It is unlikely that spatial resonance actually causes gigahertz scintillation, but it could account for the more commonly observed weaker scatter. Moreover, Rottger (1977) has suggested that the two mechanisms are complementary in that spatial resonance amplification of gravity waves can provide the input perturbation for the Rayleigh-Taylor instability.

Thus, there appear to be suitable candidate mechanisms for the production of equatorial irregularities in a localized region. However, surprisingly little is known about the morphology of irregularities on a global scale. Long-term scintillation studies from Peru have been made by Aarons (1976), from Kwajalein by Nichols (1974), and from Africa by Koster (1972). Less complete studies (in terms of seasonal dependence) have been reported by Sinclair and Kelleher (1969), and Paulson and Hopkins (1973). Generally these studies have used only one VHF or one UHF frequency in characterizing the scintillation. Taur (1973), however, has used 4- and 6-GHz signals. Taken altogether, this collection of studies gives us a wide-ranging but loosely knit sampling of the severity of amplitude scintillation at the equator as a function of frequency, time of day, season, sunspot number, geographic location, and propagation geometry.

The DNA Wideband satellite program (Fremouw et al., 1978) allows us to considerably expand our knowledge of the equatorial scintillation morphology. From stations at Ancon, Peru, and Kwajalein Atoll, both near the geomagnetic equator, satellite passes are observed over about 15° of dip latitude. The coherent CW beacons of the experiment range in frequency from VHF (137 MHz) to S-band (2891 MHz). Differential phase measurements allow us to observe the large-scale (hundreds of kilometers) structure of the ionosphere, which will be reported separately. It is the tens-of-meters-to-kilometer-sized irregularities that produce the

amplitude scintillation we will discuss here. We have statistically analyzed the scintillations at three measurement frequencies (L-band, UHF, and VHF); in conjunction with our routine weekly observations, this analysis has yielded a high-resolution seasonal morphology of the scintillation at two locations separated in longitude by ~ 120°.

This report is intended to be the first in a series using the Wideband satellite data to characterize the structure of the equatorial ionosphere. In this first report, we will deal with only one essential aspect of the problem--namely, the occurrence statistics of various levels of amplitude scintillation. We shall present cumulative effects in which the signature of single, localized irregularity regions, such as those suggested by backscatter plumes, are necessarily lost by integration with many other such regions. On the other hand, this approach provides information that the study of single, localized structures cannot--the seasonal and latitudinal variations of scintillation. This is a twofold result. First, it provides the system designer with long-term signal-fading occurrence statistics. Second, it may indicate the long-term spatial and temporal conditions under which the scintillation-producing irregularities develop, thus giving us information about the physics of the mechanism.

The results that follow are based on more than a year of Wideband data taken during the hours around local midnight when the scintillation activity peaks. This data base and the general data processing are reviewed in Section II. In Section III we show that the seasonal dependence of the scintillation at Ancon and Kwajalein is similar, with the activity centered around local summer at each location. The data have been accumulated into two sets per month, and we have found that throughout the scintillation season the activity is far from uniform. There is clear evidence of short-term variations in occurrence statistics during the active period.

We have found little difference in the magnitude or percentage of occurrence of gigahertz scintillation between Ancon and Kwajalein, contrary to an inference by Basu et al. (1976) based on a limited seasonal segment of in-situ data. However, there is a slight but systematic dif-

ference in the frequency dependence of the scintillation at the two locations, which can be attributed to differences in the respective irregularity spectra.

The latitude distributions of scintillation presented in Section IV show a systematic enhancement with decreasing elevation angle, as expected from the propagation geometry. By comparing these distributions with those predicted for uniform ionospheric irregularities, we have estimated latitudinal changes in irregularity source strength. Both Kwajalein and Ancon show an enhanced irregularity band somewhat removed from the magnetic equator that varies seasonally in location and extent.

In Section V it is suggested that neutral-wave ionization interactions are responsible for the weak-to-moderate scintillation that dominates our observations, and produces the phenomenon that we observe: the seasonal dependence of scintillation, the short-term changes in scintillation activity, and the non-equator-aligned irregularity enhancements.

We emphasize that in this report we discuss only the severity of amplitude scintillation. The important topics of second-order temporal statistics (i.e., fading rate) and spatial statistics will be discussed in future reports.

## II DATA BASE AND SATELLITE GEOMETRY

The DNA Wideband satellite was launched in late May 1976 into a 1030-km, high-inclination circular orbit for the purpose of studying transionospheric radiowave propagation. The phase of the sun-synchronous orbit is such that at low latitudes the satellite is observed on southbound passes near local midnight and northbound passes near local noon at any longitude.

The satellite transmits 10 phase-coherent CW signals: VHF (137 MHz), UHF (seven frequencies centered around 413 MHz), L-band (1239 MHz), and S-band (2390 MHz). The mutual coherence of the beacons allows us to measure phase as well as amplitude variations at each frequency. This gives us information about the full regime of ionospheric structures, ranging from large-scale total electron content variations through the kilometer-to-tens-of-meter-sized irregularities that cause the amplitude and phase scintillation. It is only these small-scale structures that we shall study in this report.

Amplitude scintillation arises from a combination of refractive and diffractive effects that a radiowave signal undergoes as it traverses the ionosphere. Fresnel filtering limits, by way of geometry and frequency, the largest electron density structure that can perturb the signal amplitude, and in effect provides an intrinsic cutoff at the low-frequency end of the amplitude frequency spectrum. In practice, while observing a moving satellite such as Wideband we see not only the signal fluctuations due to amplitude scintillation, but also longer-term variations due to spacecraft antenna pattern and free-space losses. To get a proper and unambiguous measure of the amplitude scintillation we need to remove these quasi-deterministic effects. Fortunately, the spacecraft antenna pattern is uniform enough to introduce into the amplitude record no structure with a period of less than about 30 s, and thus we have a relatively clear distinction between antenna-pattern-induced variations and the scintillation spectrum.

The separation of deterministic and scintillation components is done using the detrending process reviewed in Fremouw et al. (1978), which for amplitude is equivalent to an AGC in which the reference signal is smoothed through a sharp-cutoff low-pass filter. Empirically, 0.1 Hz was chosen early in the experiment as the detrend cutoff; removal of components with longer periods than this did not significantly effect the scintillation level. In other words, the detrend and Fresnel filter cutoffs roughly coincide.

After the scintillation component of the amplitude signal is isolated, the level of scintillation is calculated, for all Wideband analysis, in terms of the $S_4$ index (Briggs and Parkin, 1963), which is the standard deviation of signal intensity (amplitude squared) normalized to the mean intensity. The $S_4$ index ranges from near zero for an undisturbed signal to an upper limit near unity under strong scattering conditions. For the Wideband experiment, the minimum observable $S_4$ value is approximately 0.02. This limitation is due to system and sky noise.

Compared to other measures, the $S_4$ index is a preferable characterization of the level of amplitude scintillation. One advantage is that $S_4$ can be used to calculate a reasonable approximation of the probability distribution of intensity, a basic parameter of system design. To demonstrate the validity of this statement, Figure 1 shows a series of intensity distributions accumulated over approximately one minute for a variety of Wideband frequencies and scintillation levels. Superimposed are the theoretical Nakagami distributions based on the measured mean and $S_4$ of the data. These data are not selected cases except in the sense that stationary data spans were chosen. As can be seen from the figure, the Nakagami distribution provides good fits to the data over a large range of $S_4$ values independent of frequency. A more elaborate characterization of the fading statistics is discussed in Fremouw et al. (1977).

The sections that follow include observations taken during the first 1-1/2 years since satellite launch. Routine observations from Ancon (11°46'S, 77°09'W) were made between launch in May 1976 and November 1977, with periods of more concentrated data-taking during

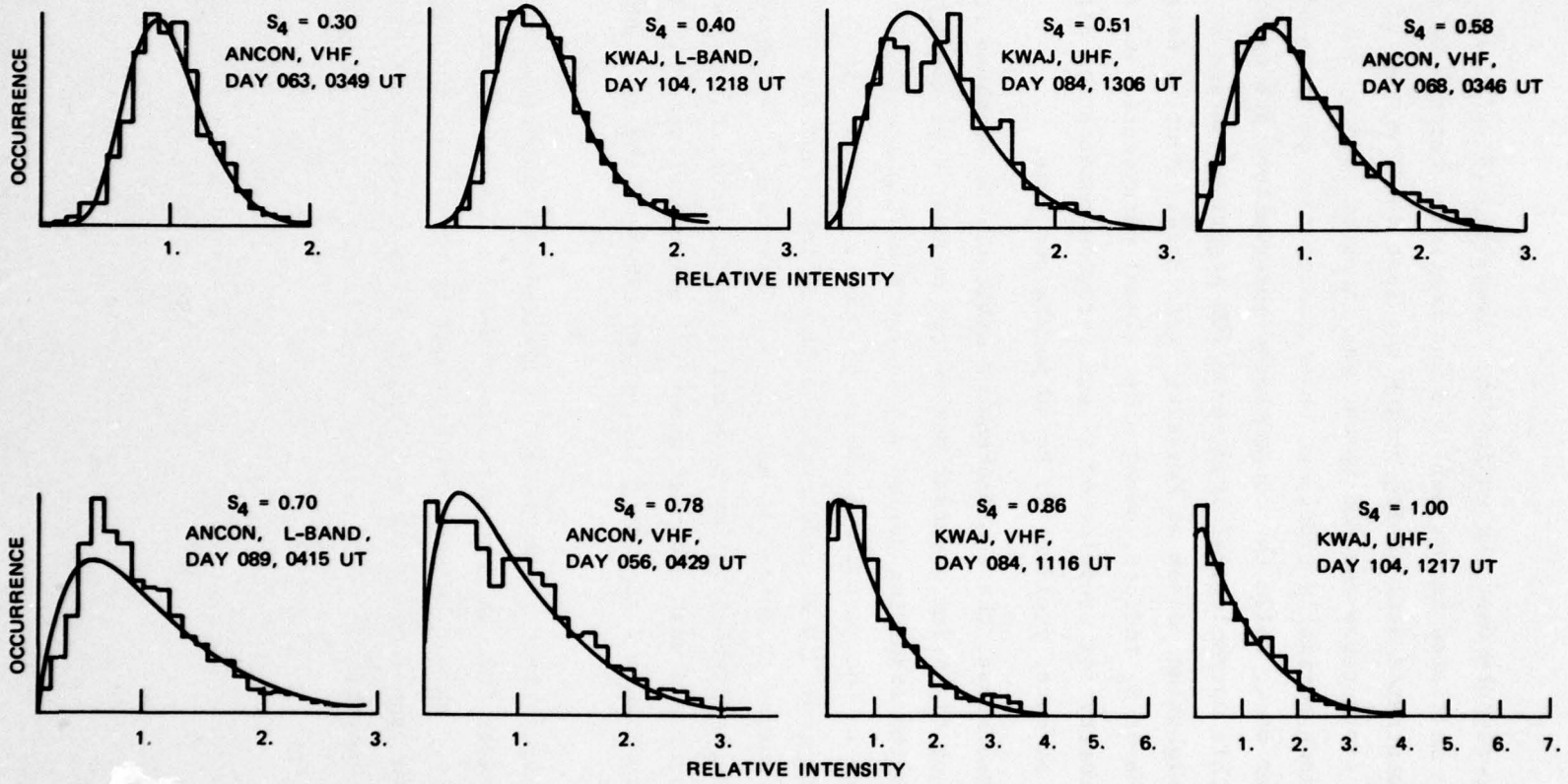


FIGURE 1 WIDEBAND EQUATORIAL INTENSITY SCINTILLATION PROBABILITY DISTRIBUTIONS AND THEIR CORRESPONDING NAKAGAMI DISTRIBUTIONS. The $S_4$ level, station, frequency, and time are indicated. All sets correspond to approximately one-minute data intervals.

coordinated experiments near the equinoxes. Kwajalein (9°24'N, 167°28'E) operations were initiated in October 1976 and continued through October 1977, with concentrated data taking during the last three months of observations. (Both sites resumed operations in early 1978.) The routine operations nominally represent three consecutive evenings of observations per week, while the concentrated observations are essentially nightly. For this morphological study some 200 nighttime passes at Ancon and 203 nighttime passes at Kwajalein were used. Routine data processing produces $S_4$ indices, among other signal parameters, and the propagation geometry for preselected E- and F-region penetration altitudes for every 20 s of data, yielding 25 to 40 points per pass.

As mentioned above, the sunsynchronous orbit of the Wideband satellite is such that nighttime observations center around local midnight. Passes early in the observing period are at low elevation angles to the east; those late in the period are low to the west. The maps in Figure 2 show typical 350-km penetration altitude locations for low and high elevation passes at Kwajalein and Ancon. Observations are often limited to a single high-elevation pass per evening; equal elevation passes to the east and west occur at about 27° maximum elevation. The marked points in Figure 2 represent the center times of the 20-s analysis segments.

Contours of constant geomagnetic dip latitude are superimposed in Figure 2 as derived from the magnetic field model (IAGA, 1969) used in routine analysis. As can be seen, symmetrical traversals of the dip equator are seen from Ancon while the Kwajalein observations are shifted slightly to the north.

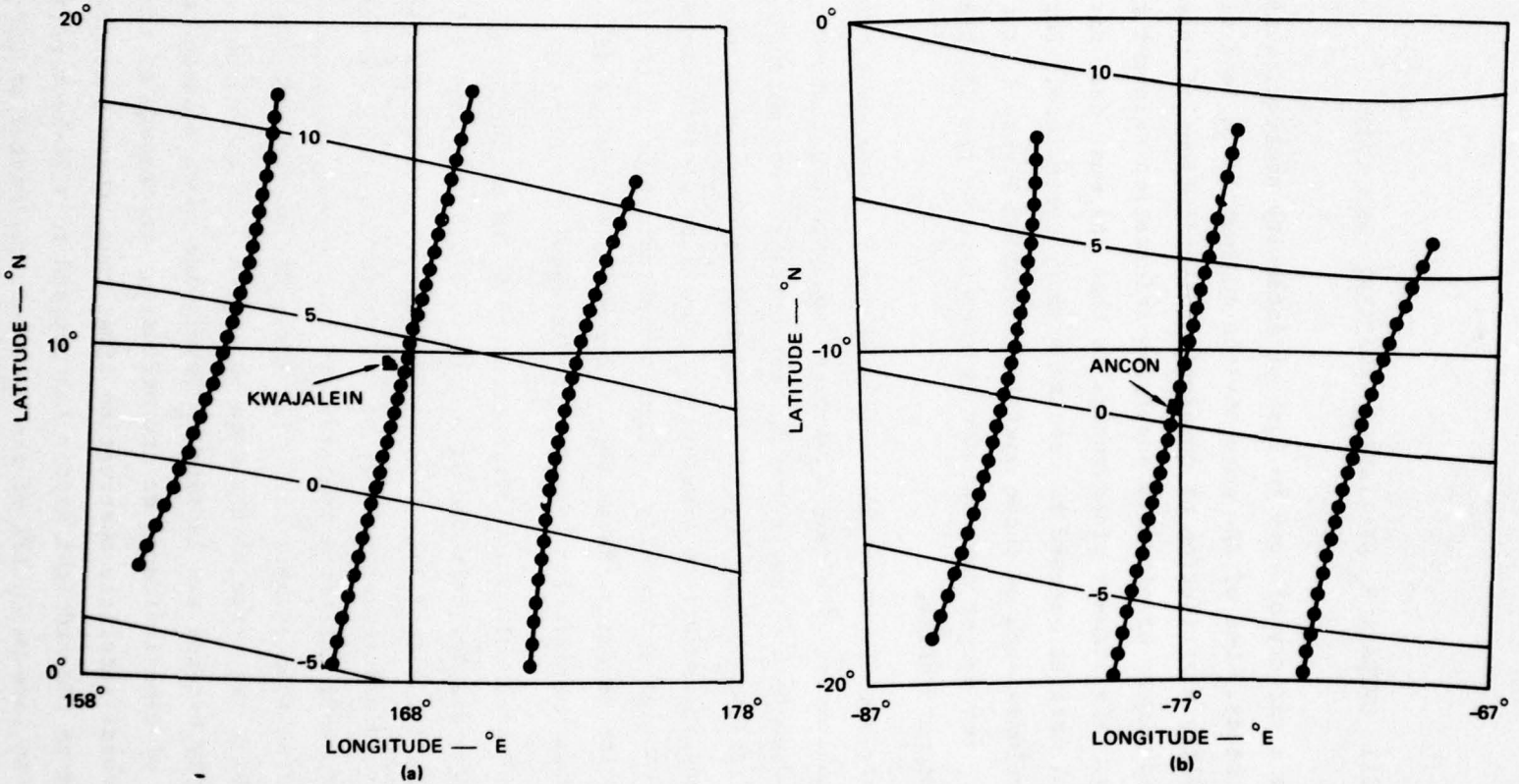


**FIGURE 2 TYPICAL WIDEBAND NIGHTTIME F-REGION (350 km) PENETRATION GEOMETRIES AT THE EQUATOR.**
The marked points are separated 20 s in time. Lines of constant dip latitude are superimposed.

## III OVERALL $S_4$ STATISTICS--KWAJALEIN AND ANCON

There are a variety of ways to look at intensity statistics in a morphological study. One of the more obvious choices is to look directly at the probability distribution or cumulative distributions of intensity. This has the advantage of directly supplying information relevant to system studies. Its primary disadvantage is that one must deal directly with the signal data as opposed to concise summary parameters. For limited data volumes such as those used in generating Figure 1, this is not a problem. For larger data volumes it soon becomes too unwieldy for useful data categorization.

We have already discussed the utility of the $S_4$ index as a scintillation level indicator. The same advantages apply to the statistics of $S_4$, and we have chosen to use cumulative $S_4$ statistics for our morphological study. Specifically, we have sorted the $S_4$ indices computed in the routine Wideband analysis into cumulative probability distributions. This yields a concise and readily interpretable indication of the long-term scintillation severity. From such information, one can easily construct intensity statistics by using the Nakagami distribution.

To display the cumulative distributions of $S_4$ in a convenient manner, we have chosen to display only the $S_4$ = 0.2, 0.4, 0.6, 0.8, and 1.0 points of each distribution. That is, we have quantized the continuous distribution into five discrete levels that we will refer to as $S_4$ exceedance levels. The seasonal data from Kwajalein in this format are shown in Figure 3 for three frequencies: VHF (137 MHz), UHF center (413 MHz) and L-band (1239 MHz). We refer to the data in Figure 3 as exceedance statistics simply because the labeled $S_4$ levels are those exceeded by the percentage of time indicated on the ordinate. Percentage of time refers to our total satellite observation time; thus, these percentages are appropriate to the midnight sector (as opposed to a 24-hour period). As an example, in late March 17% of the $S_4$ values calculated at UHF

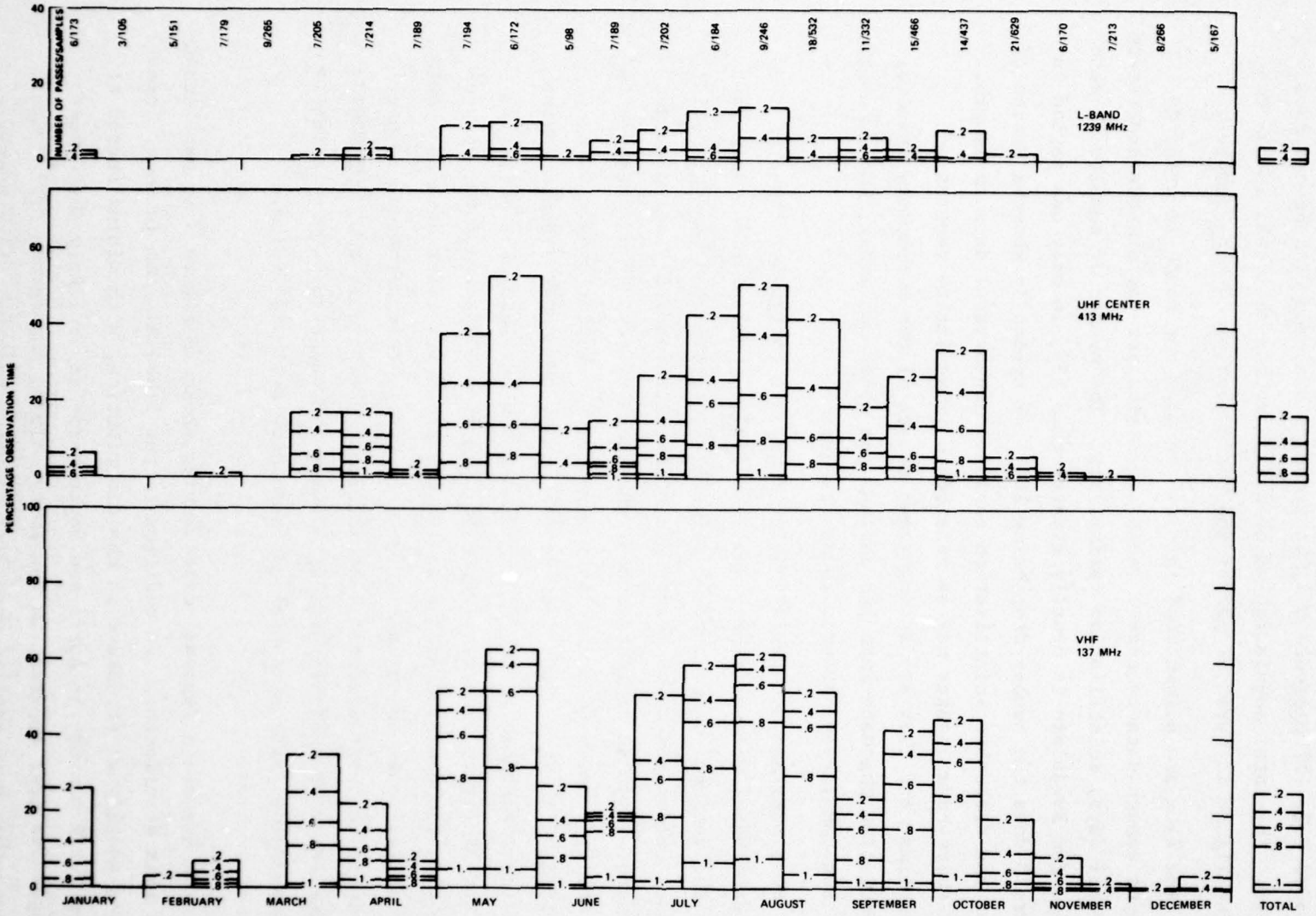


**FIGURE 3** SEASONAL DISTRIBUTION OF $S_4$ EXCEEDANCE, KWAJALEIN. The number of satellite passes and the number of 20-s $S_4$ samples used in each distribution are noted.

exceeded 0.2, 12% exceeded 0.4, 6% exceeded 0.6, and 2% exceeded an $S_4$ of 0.8. The total population of each data set is indicated in the top of the figure in terms of passes and the number of 20-s $S_4$ samples.

The data are accumulated into two periods per month in order to include enough data to ensure valid statistics yet not obscure short-term (several days) scintillation variability. The number of samples in each period for Kwajalein is usually greater than 150; in only one period in Figure 3 does the number drop below 100. We typically observe series of quiet and disturbed scintillation periods each several days in length. Such short-term changes may be related to irregularity generation mechanisms, and they are an important aspect of the morphology results. Accumulating the data into two periods per month may smear, but evidently does not completely obscure, these changes.

Some previous equatorial observations, in particular those of Koster (1968), Golden (1968), and Taur (1973), have provided data that show the seasonal dependence of scintillation dominated by equinoctial peaks. Golden generated occurrence statistics for VHF "loss-of-track" at Ancon. Because of instrumental threshold effects such a measure is not easily related to scintillation severity. Koster's data were recorded at 45 MHz. Taur recorded 4- and 6-GHz COMSAT signals. More directly comparable to the Wideband data are the later Koster (1972) and Aarons (1976) observations at 137 MHz from Ghana and Peru, respectively. Although both Aarons and Koster interpret their data as showing equinoctial peaks in scintillation occurrence, that signature is not prominent in their seasonal distributions. We suggest that one could better describe their results as showing a broad 8-to-9-month scintillation season, with a central but secondary activity medium.

The Kwajalein seasonal distribution shown in Figure 3 is consistent with this description. In addition to the broad minimum in June, however, we see additional structure in the distribution, with minima spaced at about 2-1/2 months, in April and September. It is likely that these changes are less apparent in the Koster (1972) and Aarons (1976) data, because they have applied smoothing to their seasonal distributions.

These variations in activity generally track from one frequency to the next. In fact, the seasonal behavior of the exceedance levels compares well at two frequencies that correspond to roughly the same degree of scattering. For example, this is the case with VHF (UHF) $S_4 > 0.8$ compared to UHF (L-band) $S_4 > 0.2$. On the other hand, changes in weak-scatter exceedance levels ($S_4 > 0.2$, 0.4) at the three frequencies do not always match. This is seen most clearly in Figure 3 during the March-April and September periods, where the scintillation trends at VHF and L-band are in opposite directions. In September, for instance, at L-band the scintillation decreases, at UHF all levels remain relatively constant, and at VHF the scintillation occurrence increases. In Section V we suggest that both the variability of scintillation activity and these structural differences in the occurrence statistics between frequencies are related to systematic changes in irregularity onset and generation.

Gigahertz scintillation, which we have somewhat arbitrarily chosen to call L-band $S_4$ values greater than 0.2, persists throughout the summer at Kwajalein and is seen more than 10% of the time in July and August. It is generally accompanied by near-saturated scintillation at UHF and an always-saturated disturbance at VHF. However, saturated scintillation at VHF does not guarantee the existence of gigahertz scintillation. The necessity for a beacon with frequencies ranging above 1 GHz to characterize the amplitude scintillation morphology is obvious under these conditions.

The yearly totals of scintillation exceedance are shown to the right of Figure 3. These were calculated from equal weighting of the 24 data segments rather than the percentage of passes, in order to avoid a bias toward the periods of intensive observations. The results give some idea of the overall occurrence of nighttime equatorial scintillation for minimum solar activity.

The corresponding $S_4$ exceedance levels for Ancon are shown in Figure 4. Note that there has been a six-month shift in the time axis with respect to the Kwajalein figure. As with Kwajalein, the scintillation activity persists throughout the local summer (January) and ceases during the local winter (July). The reason for a simple six-month shift in the activity for stations in opposite hemispheres has not been adequately explained, and will be briefly discussed in Section V.

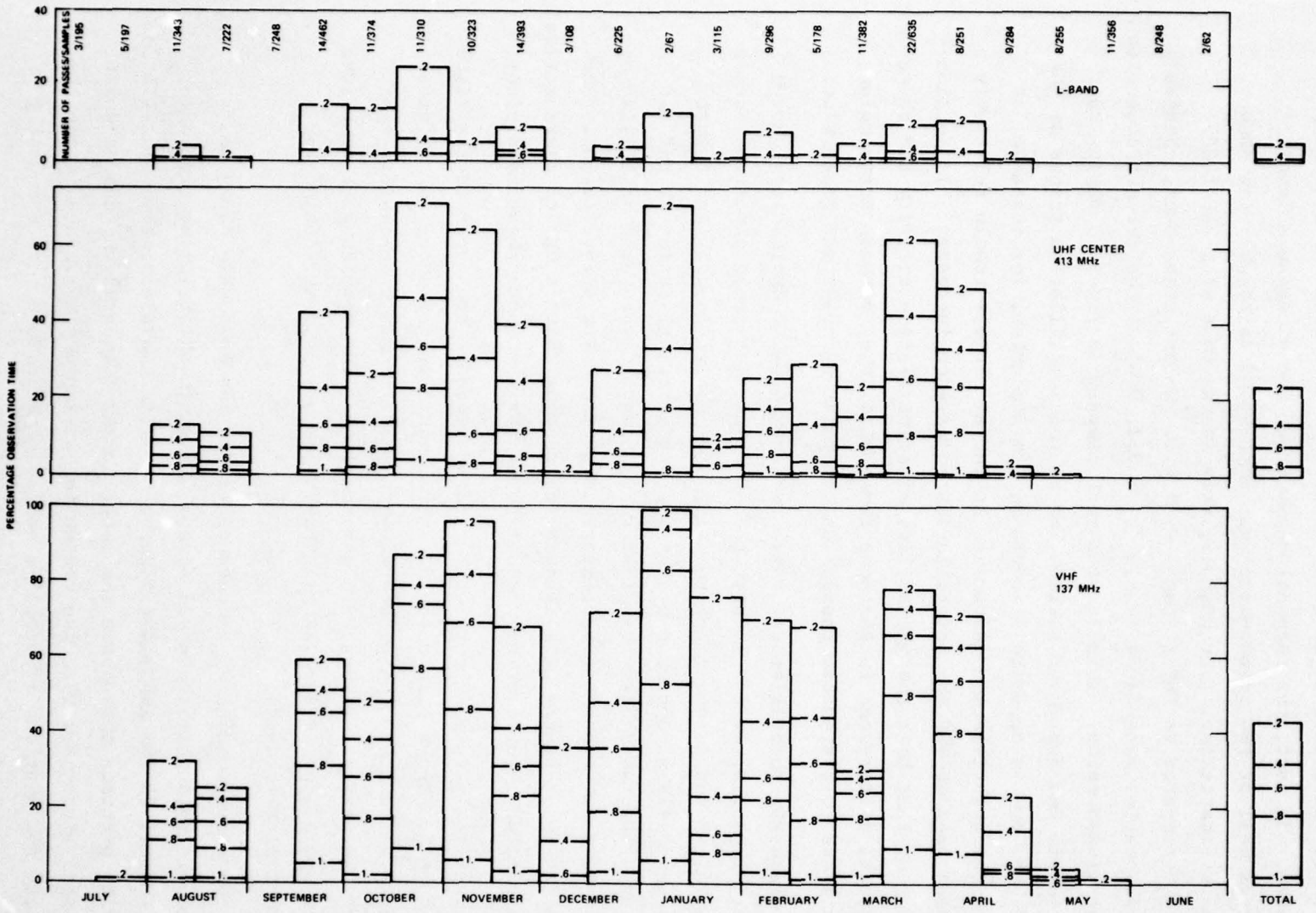


**FIGURE 4** SEASONAL DISTRIBUTION OF $S_4$ EXCEEDANCE, ANCON. The number of satellite passes and the number of 20-s $S_4$ samples used in each distribution are noted.

The Ancon data show short-term variations in occurrence statistics that are qualitatively similar to the Kwajalein data. Indeed, in the VHF occurrence statistics, minima occur at regular 3-month intervals. We also see similar structural dissimilarities in the occurrence distributions at VHF, UHF, and L-band frequencies. These are more pronounced than those in the Kwajalein data, and occur in the November and February-March periods. During these times, the occurrence of gigahertz scintillation increases while all but the strongest scatter levels at VHF decrease.

Despite these similarities between Figures 3 and 4, there is a major difference: while the occurrence statistics of gigahertz scintillation at Kwajalein and Ancon are nearly identical when shifted relative to one another by six months, Ancon shows considerably more VHF and UHF scintillation. To show this quantitatively, we need only compare the cumulative statistics. At Ancon, for example, $S_4$ at VHF exceeds 0.2 43% of the time, whereas the corresponding figure for Kwajalein is only 26%. The $S_4$ 0.2 exceedance at L-band for the two stations differs by less than 1%.

This difference in the frequency dependence of $S_4$ between the stations is consistent with the findings of a recent study by Rino and Matthews (1978). They found a systematic difference between the average spectral index measured from the Kwajalein UHF and VHF phase data, and the corresponding Ancon data. The phase spectral density function has the general power law form $f^{-p}$, where f is frequency, and p is spectral slope. For the Ancon data, Rino and Matthews deduced an average p value near 3, as is generally accepted. For the Kwajalein data, however, the average p index was closer to 2.5. For a uniform power-law medium under conditions of weak to moderate amplitude scintillation, $S_4 \propto f^{-(p+3)/4}$. Thus, if p = 3, then $S_4 \propto f^{-1.5}$; and if p = 2.5, then $S_4 \propto f^{-1.38}$. In Figure 5 we compare the frequency dependences deduced from the yearly average $S_4$ cumulative distributions.

The vertical bars indicate the separation of $S_4$ levels between a pair of frequencies at the same percentage of exceedance. The levels of 0.5 and 0.7 were chosen for comparison so that the $S_4$ values measured at the lower frequency would remain above $\sim$ 0.1 because below this value

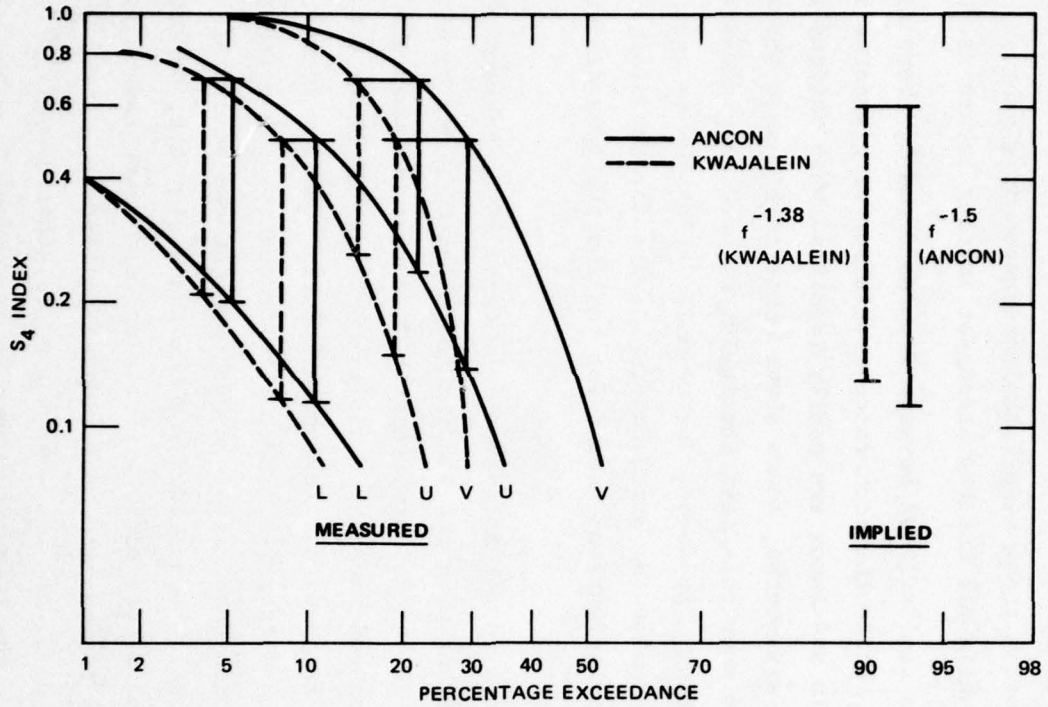


FIGURE 5 TOTAL $S_4$ CUMULATIVE DISTRIBUTIONS AT ANCON (solid) AND KWAJALEIN (dashed). The vertical bars indicate measured and phase-spectrum implied $S_4$ dependence.

the distributions are rather uncertain. Since multiple-scatter effects are important for $S_4$ values greater than 0.4, the length of the vertical bars will underestimate the actual spectral slope. Theoretically implied frequency dependences are shown on the right-hand side of the figure for comparison. We see that while the exact spectral slope cannot be accurately estimated, the Kwajalein data are clearly consistent with a more shallowly sloped spectral distribution of irregularities than the Ancon data.

Before going on to the latitudinal distribution of scintillation it is worthwhile to compare Wideband seasonal statistics with data collected at Kwajalein and Ancon by other experimenters. At Kwajalein, Nichols (1974) observed a geostationary satellite at 254 MHz during 1971 and 1972, a period of somewhat higher sunspot number (SSN $\sim$ 60) than the Wideband data period (SSN $\sim$ 20). Nichols presents his data in terms of 5- and 10-dB amplitude fading exceedances, and we have tried to relate these data to the Wideband 413-MHz $S_4$ statistics using appropriate frequency dependences and the fading/SI/$S_4$ conversions of Whitney (1974). Either because of saturation effects or non-applicability of the conversions, the quantitative agreement is poor and the extrapolations severely underestimate the scintillation levels measured by Wideband. Nonetheless, the seasonal variation of the Wideband data agrees with the seasonal variation of the Nichols' data, as can be seen in Figure 6 where the monthly accumulation of Wideband 413 MHz data with $S_4 > 0.6$ is superimposed on Nichols' data.

The Peru data discussed by Aarons (1976) are better suited to direct Wideband Ancon comparison. His data at 137 MHz from ATS-3 were collected between August 1973 and July 1974, a period of sunspot number similar to the 1976-1977 Wideband period. Aarons presents his data in terms of percentage exceedance of SI > 60, which converts to $S_4 > 0.3$ (Whitney, 1974). The seasonal SI data for times near local midnight are compared with monthly accumulations of the Wideband $S_4 > 0.3$ exceedances in Figure 7. The two data sets agree both quantitatively, in terms of scintillation exceedance and in the general seasonal dependence of activity. Note, however, that most evidence of the scintillation short-

term variability so clear in the VHF data of Figure 4 is effectively hidden in the monthly accumulations.

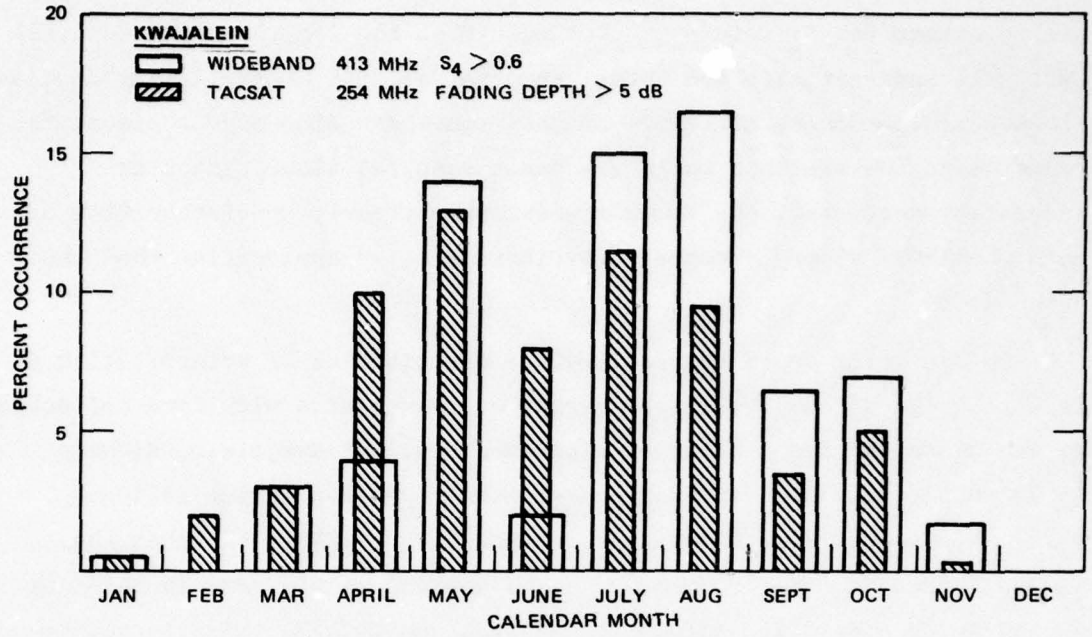


FIGURE 6 COMPARISON OF TACSAT AND WIDEBAND SCINTILLATION CHANGES WITH SEASON AT KWAJALEIN. No quantitative comparison of the scintillation severity is implied.

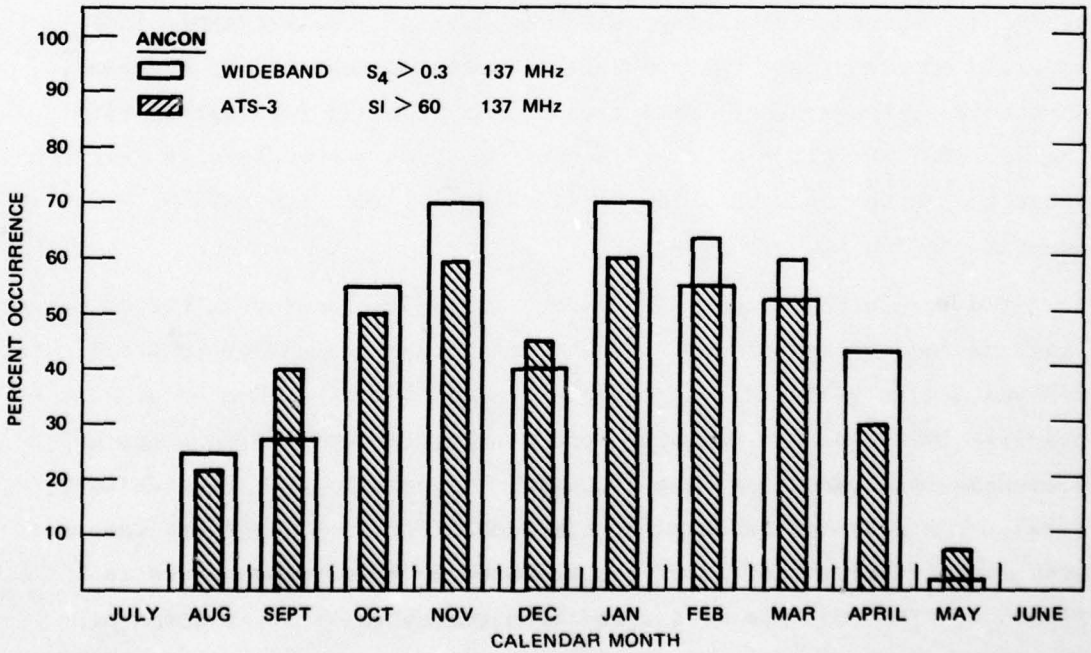


FIGURE 7 COMPARISON OF ATS-3 AND WIDEBAND SCINTILLATION SEVERITY AND SEASONAL DEPENDENCE AT ANCON

## IV LATITUDINAL DISTRIBUTION OF SCINTILLATION--KWAJALEIN AND ANCON

We have seen in the previous section that the seasonal behavior of scintillation at Kwajalein and Ancon is similar, although shifted six months, while the severity of scintillation at VHF and UHF frequencies is systematically different. In this section, we investigate the latitudinal distribution of the scintillation at each site.

The behavior of scintillation with latitude should yield some information about the irregularity generation mechanism or mechanisms. For example, if the Rayleigh-Taylor instability dominates, a broad band of irregularities, symmetrical about the equator, should be seen. This is where the flux tubes over which the instability acts are highest in altitude and the least collision-dominated. On the other hand, a mechanism like spatial resonance depends upon the direction of neutral waves with respect to the local magnetic field. Because the field declinations are not uniform over the region we observe (Figure 2), a dominant neutral wind or plasma drift direction might produce preferred regions of irregularity occurrence, not necessarily centered on the geomagnetic equator.

Experimentally, an approximately ± 25° geomagnetic latitude spread-F band is seen about the magnetic equator in ionosonde studies, both bottomside (Wright, 1959) and topside (Calvert and Schmid, 1964). Several studies have also been made of the latitude distribution of scintillation, yet little definitive data is available. Sinclair and Kelleher (1969) using moving beacons at 40 MHz in the African sector in 1966-1967 observed a southern limit to the scintillation band at about -25° geomagnetic latitude. The northern extent of the measurements was +5° geomagnetic, and no northern boundary was seen. The same data indicate some minor variations in the width of the scintillation band with season and magnetic activity. Nearly simultaneous (1967-68) studies in Peru using the same two 40-MHz beacons (Chatterjee et al., 1974) found

a much narrower band of about ± 10° about the magnetic equator. The experimenters suggest that this indicates a true longitudinal difference in the scintillation band between the stations. The discrepancy may be in part due to the difference in instrumentation, data processing, and local observation times used in the two experiments. Later on, we will comment further about the data interpretation used in both of these experiments.

Taur (1973) has presented scintillation at 4 and 6 GHz for geostationary sources. Using weak fading occurrences at 13 stations distributed worldwide within ± 30° of the equator, he finds no simple scintillation dependence on latitude. A scintillation band of sorts can be fitted to his data over about ± 25° of geomagnetic latitude. Paulson and Hopkins (1973), who also used geostationary sources, saw a decrease in the occurrence but not in the severity of scintillation at 17.5° geomagnetic north relative to stations at the magnetic equator. However, their total observation time was too short and the longitudinal separation of their stations too large to exclude seasonal variations as causing some of this decrease. They also explored elevation-angle dependences for a series of geometries, seeing no significant effects. Again, short observation times and the often-localized occurrence of equatorial scintillation leave this result in doubt. All in all, little can be concluded from these previous studies except that a limited scintillation band within ± 10° to ± 25° of the geomagnetic equator has been observed.

The high inclination of the Wideband orbit provides an opportunity to observe multifrequency scintillation over about 20° of geographic latitude near the equator at F-region penetration altitudes. For lower elevation passes, curvature of the earth shortens this latitude range and accounts for the curvature in the penetration locations seen in Figure 2. An advantage of the moving beacon for latitudinal studies is that we get a snapshot of the true spatial distribution of scintillation (modified by propagation geometry) smeared only by 10-to-14 minutes of temporal change.

In analyzing scintillation distributions using a moving beacon such as Wideband, any true spatial changes in source occurrence will be complicated by propagation effects. Diffraction theory predicts an enhancement of scintillation level with decreasing elevation angle, which is due to the lengthening of the propagation path. Thus, a uniform scattering layer of isotropic irregularities will produce variations in $S_4$ index proportional to sec $\theta$, where $\theta$ is the local zenith angle of the propagation path in the layer. At the equator, where the irregularities are typically elongated with axial ratios larger than 10:1 (Rino and Livingston, 1978), the geometrical dependence is more complicated. In effect, the $S_4$ enhancement at the horizons decreases somewhat with increasing axial ratio, reaching a lower limit for elongations beyond about 30:1. Even at high axial ratios, however, the median $S_4$ at high elevation angles due to a uniform scattering layer may be half that observed at the horizons. Clearly, proper interpretation of the latitudinal scintillation distribution in terms of irregularity source regions will require evaluation of these propagation effects.

In accumulating the latitudinal distributions, we have continued to use the cumulative distribution of $S_4$ index, at least as a starting point. We have also chosen to work with only the VHF and UHF data, since the higher $S_4$ levels at UHF ($S_4 \sim 0.8$) generally track the lower $S_4$ levels at L-band ($S_4 \sim 0.2$). Four exceedance levels, $S_4 > 0.2$, 0.4, 0.6, and 0.8 have been retained in order to study, to the extent possible, the latitude distribution of scintillation for a range of scattering conditions.

In the latitudinal studies, the same sample population used in the total statistics is now spread over a large range of latitudes, and to retain statistical validity, longer accumulation spans are necessary. Biweekly and monthly spans were tried, but simply reflect the basically patchy nature of the equatorial ionosphere. Localized latitudinal preferences can be identified in the monthly accumulations, but are not systematic from month to month; such short-term preferences are not really appropriate to this morphological study and will be treated elsewhere.

Three-month accumulation spans were finally chosen--September-November/February-April at Ancon and March-May/August-October at Kwajalein. These give us the required statistical populations within the 1° (geographic) latitude resolution we wish to analyze, mostly because they bracket periods of concentrated data collection. At the same time, by looking at fall and spring data separately, we should see indications of seasonal changes, if any, in the scintillation-belt width or location. For comparison, we have also accumulated latitudinal distributions for the total eight-month scintillation season at each site, March-October at Kwajalein, and September-April at Ancon.

For all distributions we have limited the analysis to a central 13° geographic latitude band for F-region (350 km) penetration locations over which the sample population is nearly uniform. The data are sorted into one-degree geographic bins. Sorting the distributions according to geographic latitude was chosen because of advantages in the data processing, and because we did not want to assume that the scintillation band is geomagnetically centered. Because of the nonzero declination of the magnetic field at Kwajalein and Ancon this will broaden the distribution signature of a feature fixed in geomagnetic latitude but extended in longitude. Figure 2 shows that the maximum smearing is about two (geographic) degrees over the full longitudinal extent of F-region penetrations. This should be a negligible effect with adequate statistical sample populations.

The resulting latitudinal distributions of four $S_4$ exceedance levels at UHF and VHF at Kwajalein are shown in Figure 8. Data for the two three-month spring-fall and total scintillation seasons are given. The ordinate of each box is percentage of total observation time and each column corresponds to one degree in geographic latitude at a 350-km penetration altitude. The dip latitude scale corresponds to a near-overhead pass at the station; because Kwajalein is located at nearly 5° dip latitude, we observe farther north, than south, of the dip equator.

One important feature in Figure 8 is the difference between the distributions corresponding to strong and weak scattering. The stronger scattering distributions (e.g., UHF $S_4 > 0.6$) show an increased occurrence

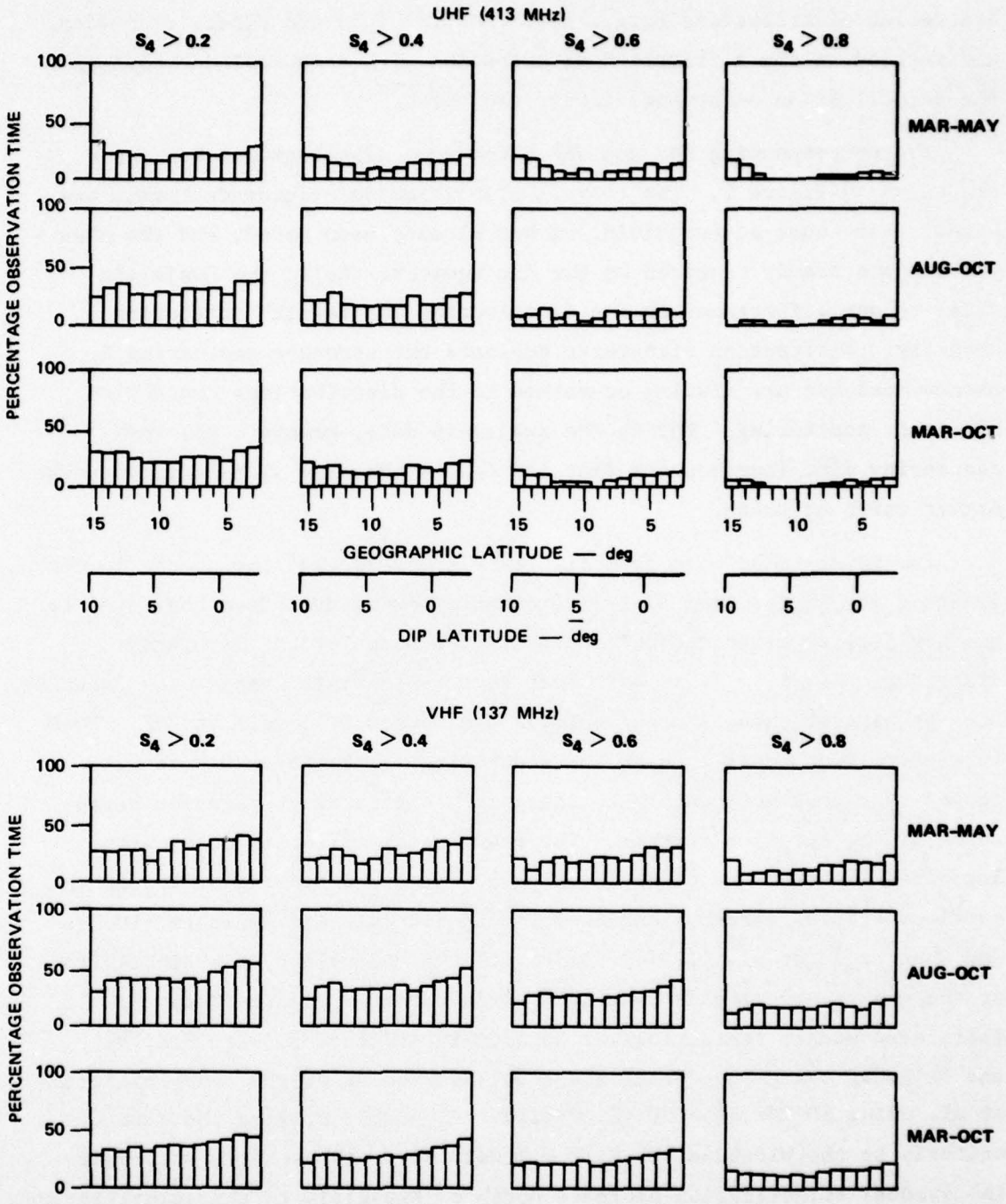


FIGURE 8 LATITUDINAL DISTRIBUTIONS OF $S_4$ EXCEEDANCE AT KWAJALEIN, AT UHF AND VHF FREQUENCIES, 350-km PENETRATION ALTITUDE. Data for two three-month spring and fall periods and the eight-month main scintillation season are shown,

of scintillation toward the edges of the distribution (lower elevation angles), as would be expected from diffraction effects. In the weaker scattering distributions (e.g., VHF $S_4 > 0.2$) the same effect is hidden, and instead we see a flattened distribution with a general decrease in the scintillation occurrence toward the north.

The corresponding UHF and VHF exceedance distributions for Ancon are shown in Figure 9. The overall scintillation occurrence levels are higher than those at Kwajalein, as has already been noted, and the observations are nearly centered on the dip equator. As in the Kwajalein data, we see differences in the distribution shapes with scattering severity. Diffraction signatures dominate the stronger scattering $S_4$ exceedances but are missing or masked in the distributions controlled by weaker scattering. Unlike the Kwajalein data, however, the weak-scattering distributions are flat and do not show any systematic decrease either north or south.

The point to be made from Figures 8 and 9 is that the change in the shape of the latitudinal distribution of $S_4$ exceedance from one level to another implies a latitudinal change in the shape of the cumulative distribution of $S_4$. It is not clear what causes this change with latitude, but the biggest changes occur between the lowest $S_4$ levels at VHF. Thus, it appears that there is weak VHF scattering (in the $S_4 \sim 0.2$ to 0.4 range) that does not conform to the same geometrical propagation dependence as the stronger scatter. The changing distribution of $S_4$ with latitude, whatever the cause, does point out a shortcoming of two of the previous studies already mentioned. Both Sinclair and Kelleher (1969) and Chatterjee et al., (1974) dealt with the equivalent of a single frame of the weak scattering exceedance distributions in Figures 8 and 9. In fact, even weaker scattering was used in those studies, with Sinclair and Kelleher using any detectable scintillation at 40 MHz, and Chatterjee et al. using 40 MHz SI > 30 ($S_4 \geq 0.2$). If we had applied the same criteria to the Wideband VHF $S_4 > 0.2$ data we would probably attribute the gradual scintillation decrease north of Kwajalein to the scintillation band boundary. The flat distribution at Ancon would be interpreted as a uniform scintillation band centered on the equator. When we consider our data overall, however, we find that this is not a valid interpretation.

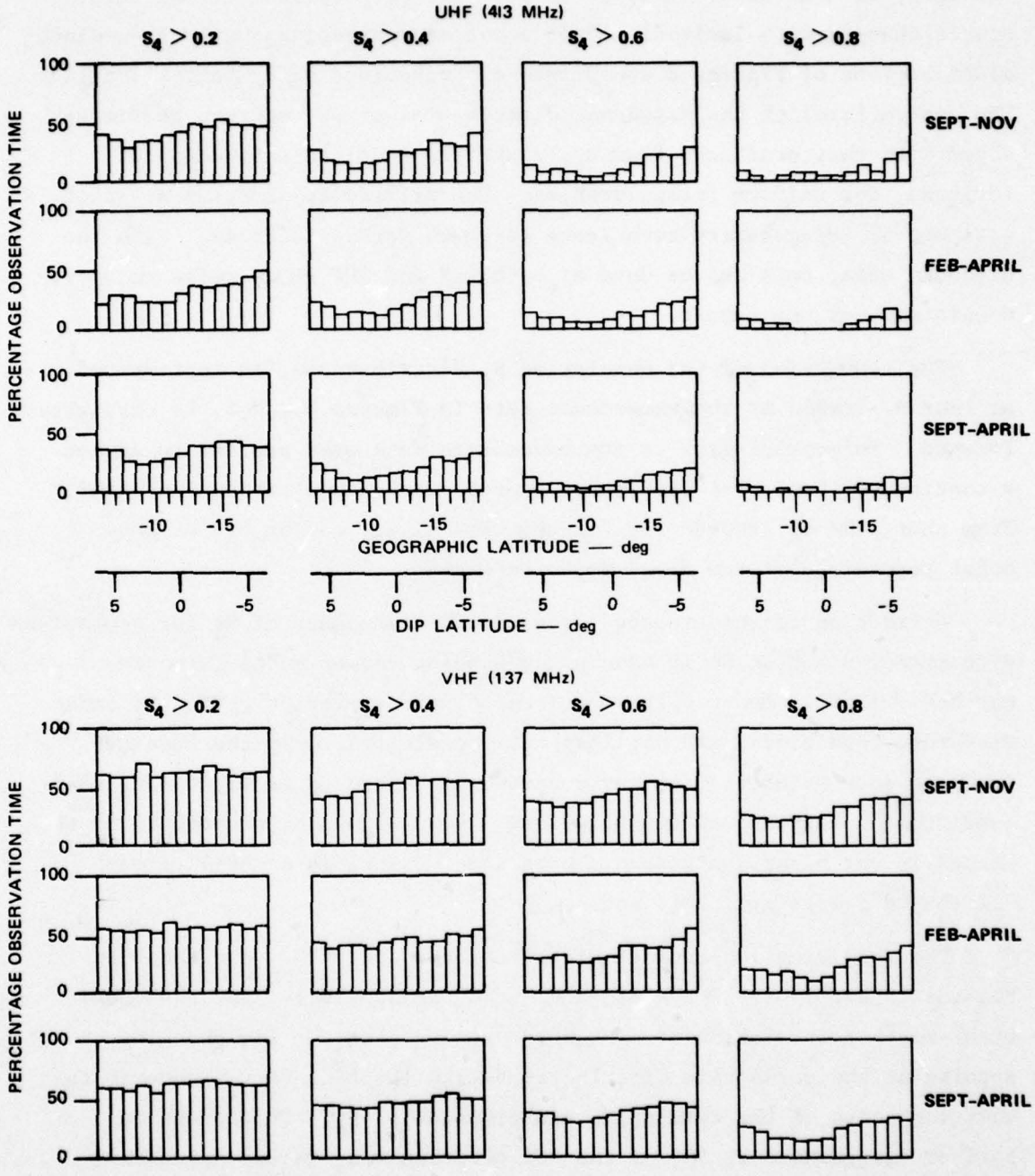


FIGURE 9 LATITUDINAL DISTRIBUTIONS OF $S_4$ EXCEEDANCE AT ANCON, AT UHF AND VHF FREQUENCIES, 350-km PENETRATION ALTITUDE. Data for two three-month spring and fall periods and the eight-month main scintillation season are shown.

There is a far better approach to sorting scintillation versus latitude, and one that allows us to more directly estimate irregularity source changes with latitude. This involves converting the $S_4$ exceedance distributions of Figures 8 and 9 into distributions of $S_4$ versus latitude. The median level of the resulting distribution of $S_4$ can then be differenced with that predicted from a propagation model as a function of latitude, for uniform irregularities. The difference gives us a direct estimate of irregularity turbulence strength versus latitude. With the Wideband data, this can be done at both UHF and VHF frequencies to verify consistency of the result.

The conversion of the cumulative $S_4$ distributions, as represented at four $S_4$ levels by the exceedance data in Figures 8 and 9, is straightforward. Polynomial fits to the exceedance data were applied to derive a continuous cumulative distribution of $S_4$ for each latitude increment. From that, the $S_4$ exceeded 50% of the time (i.e., median $S_4$) or any other percentage of the time may be extracted.

Estimation of the expected geometrical dependence of $S_4$ for comparison with measured median $S_4$ is made using a phase screen model (Rino and Matthews, 1978). Because the model calculations predict median $S_4$ under disturbed conditions, and not long-term conditions, only the evenings in which some scintillation was observed were used to recreate disturbed-condition $S_4$ latitudinal distributions. For Kwajalein, about half of the passes in our eight-month span showed some measurable scintillation; 73% showed scintillation at Ancon.

The resulting latitudinal distributions, now of $S_4$, are shown in Figures 10 and 11 for Kwajalein and Ancon, respectively, for the total eight-month accumulation of disturbed evening passes. The changing spacing of the percentile distributions with latitude corresponds to the changing shape of the cumulative distribution of $S_4$. This shape is further exaggerated at VHF as the 40% occurrence $S_4$ values approach strong scatter ($S_4 \geq 0.7$).

Superimposed on each set of curves in Figures 10 and 11 is the predicted median $S_4$ calculated from the phase screen model for the

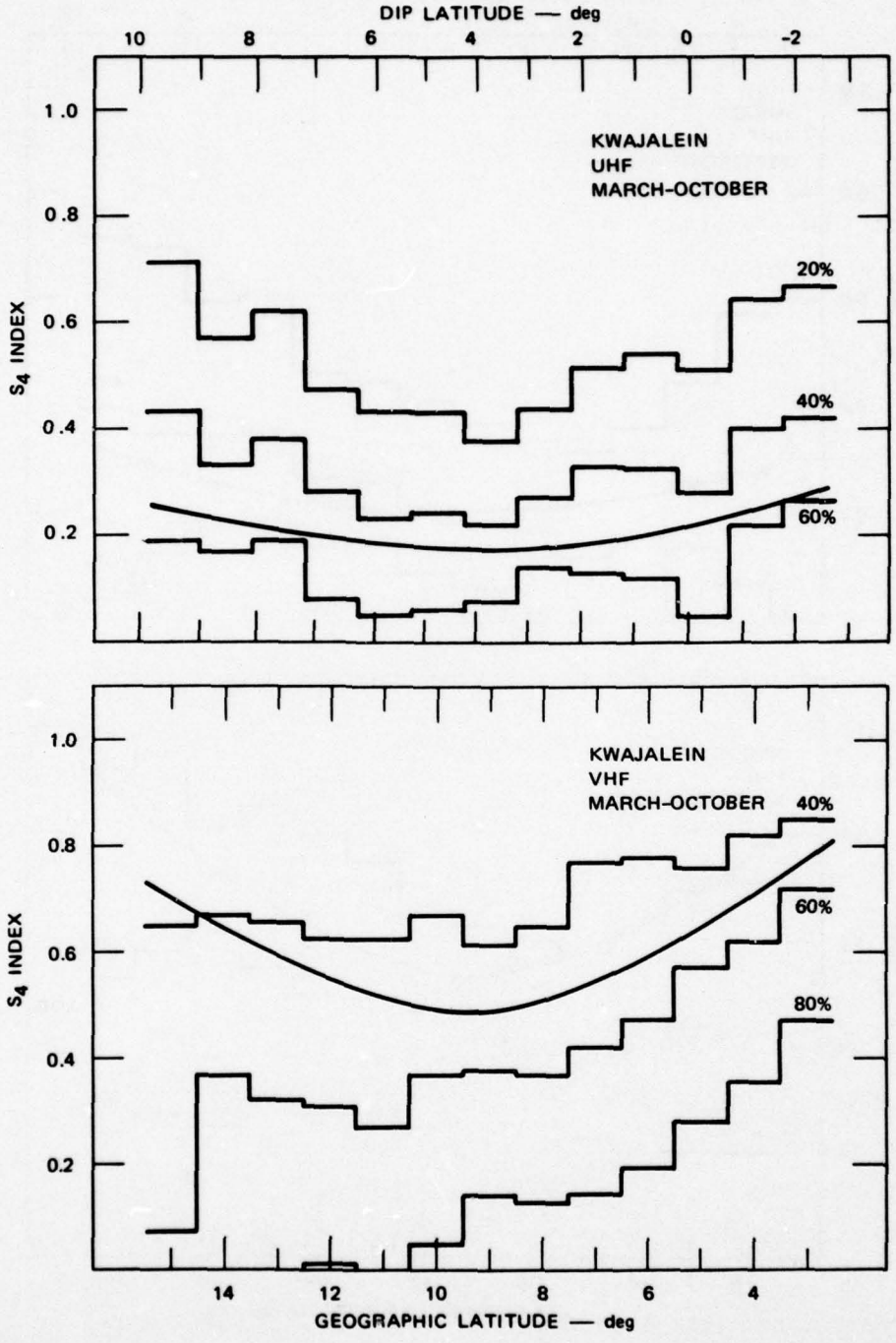


FIGURE 10 LATITUDE DISTRIBUTION OF $S_4$ AT KWAJALEIN IN TERMS OF PERCENTILE OCCURRENCE AT UHF AND VHF FREQUENCIES, DISTURBED PASSES ONLY. Also shown is the median $S_4$ predicted from the phase-screen model assuming a uniform distribution of ionospheric irregularities.

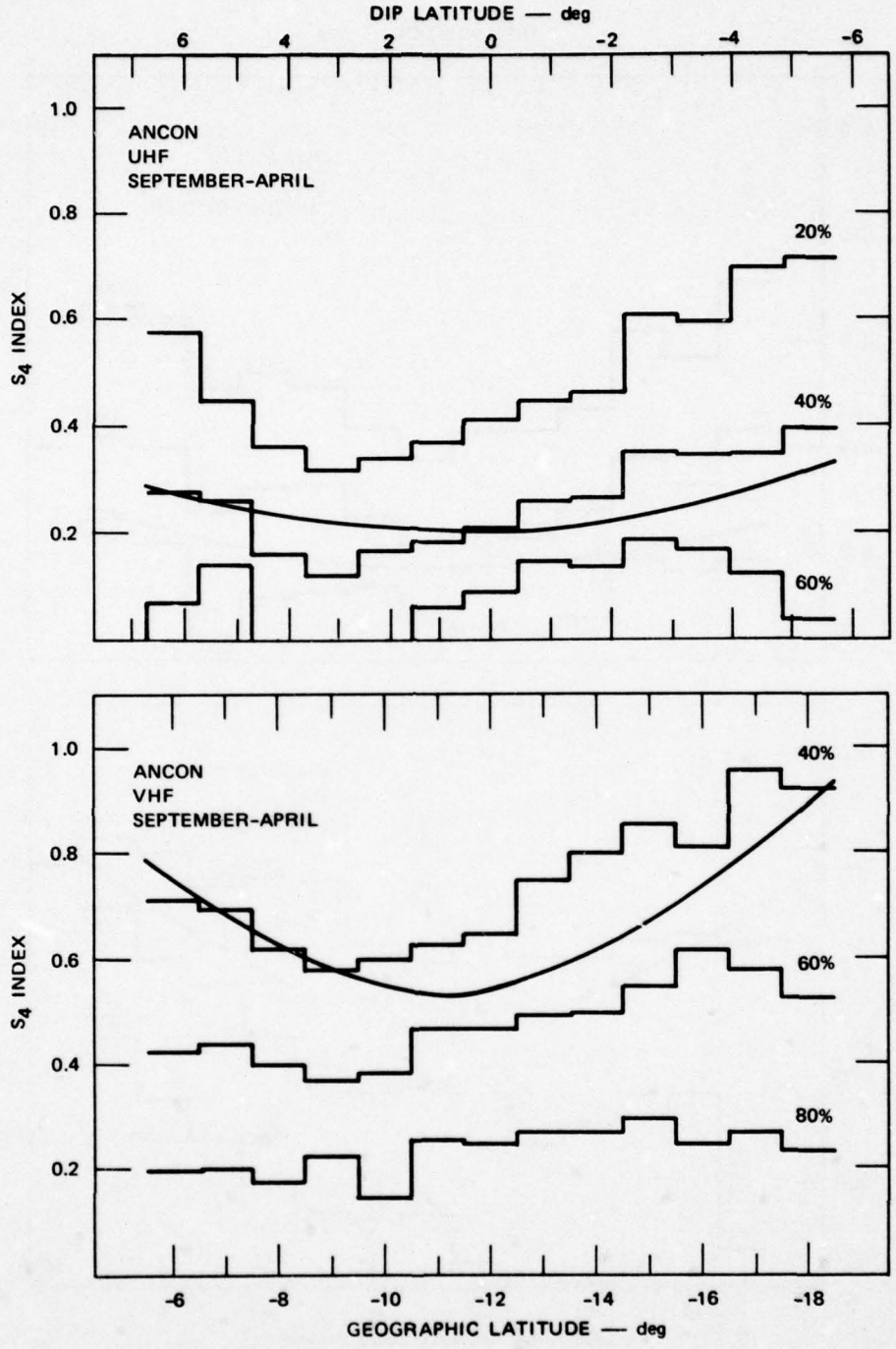


FIGURE 11 LATITUDE DISTRIBUTION OF $S_4$ AT ANCON IN TERMS OF PERCENTILE OCCURRENCE AT UHF AND VHF FREQUENCIES, DISTURBED PASSES ONLY. Also shown is the median $S_4$ predicted from the phase-screen model assuming a uniform distribution of atmospheric irregularities.

appropriate ionospheric parameters and turbulence model. It represents the long-term median $S_4$ versus latitude we would expect to see for a uniformly distributed and unchanging screen of F-region irregularities. Field-aligned irregularities of axial ratio 20:1 have been assumed, although the predictions are relatively insensitive to irregularity elongation; the predicted $S_4$ values change only 1-to-2% between isotropic irregularities and those with a 100:1 axial ratio.

To specify the in-situ turbulence within the phase-screen model, irregularity spectral slope and strength of turbulence must be specified. The slopes used correspond to the same $p = -2.5$ and $p = -3$ phase slope values for Kwajalein and Ancon, respectively, that were discussed in Section III as appropriate for the observed $S_4$ frequency dependences. The turbulence strength has been adjusted (somewhat arbitrarily) to roughly match, at its minimum, the measured median VHF $S_4$.

The final specification for the phase screen model is pass geometry. We have a relatively uniform distribution of pass geometries between the low-elevation passes shown in Figure 2, and overhead. The predicted median $S_4$ in Figures 10 and 11 is an average of the predictions for the three pass geometries shown for each station in Figure 2. It should be within a few percent of the median $S_4$ we would have obtained by averaging the phase screen outputs for each of the many passes used in the analysis.

If we now compare the model-measurement fits for Kwajalein in Figure 10, we find good agreement for UHF and fair agreement for VHF, where the measured $S_4$ drops below that predicted in a region to the north. For Ancon, in Figure 11, the measured data match the prediction well only to the south. Thus, at neither site do we see consistently good agreement between the overall (8 month) measured scintillation distributions and those predicted for uniform ionospheric irregularities.

We next consider whether these discrepancies between the measured and predicted data continue to be seen for the three-month spring-fall data sets. They do, both in the Kwajalein and Ancon data, which are shown in Figures 12 and 13. In these figures, only the median measured $S_4$ is now shown; for easier comparison with the theoretical curve, a least-squares polynomial fit (fourth-order) has been made to the data,

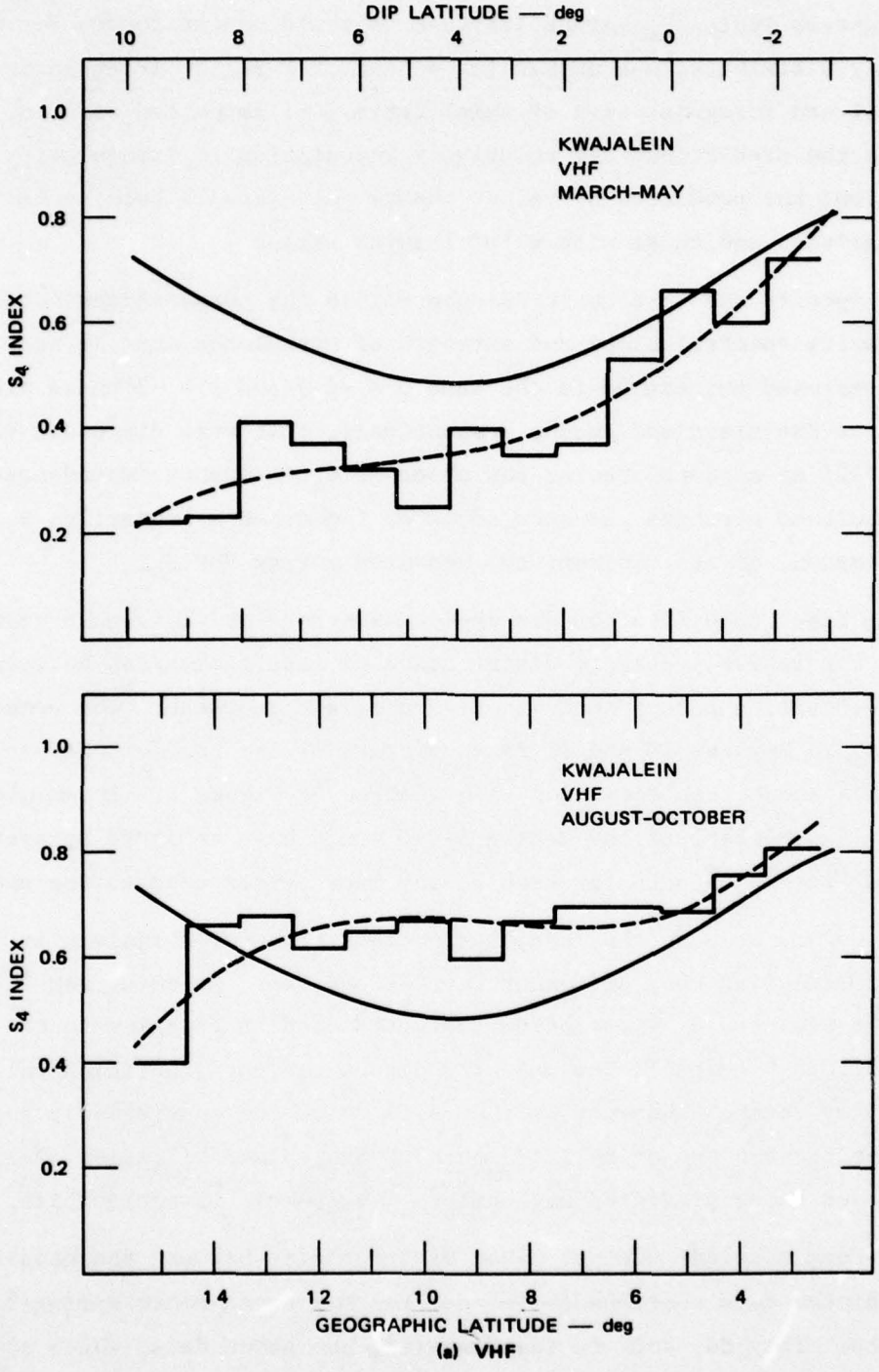


FIGURE 12 LATITUDE DISTRIBUTIONS OF MEASURED AND PREDICTED MEDIAN $S_4$ AT KWAJALEIN, SPRING AND FALL PERIODS

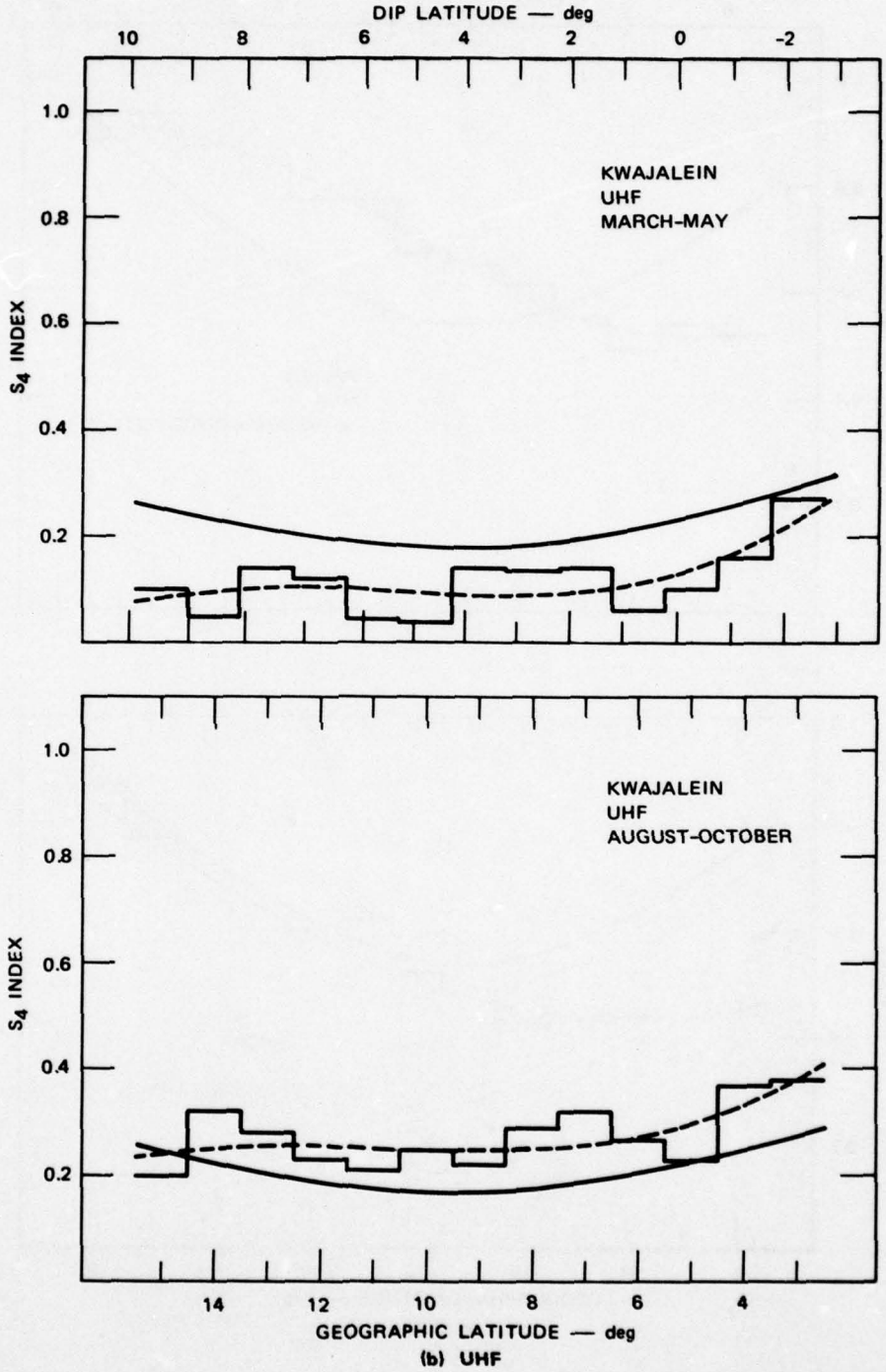


(b) UHF

FIGURE 12 (Concluded)

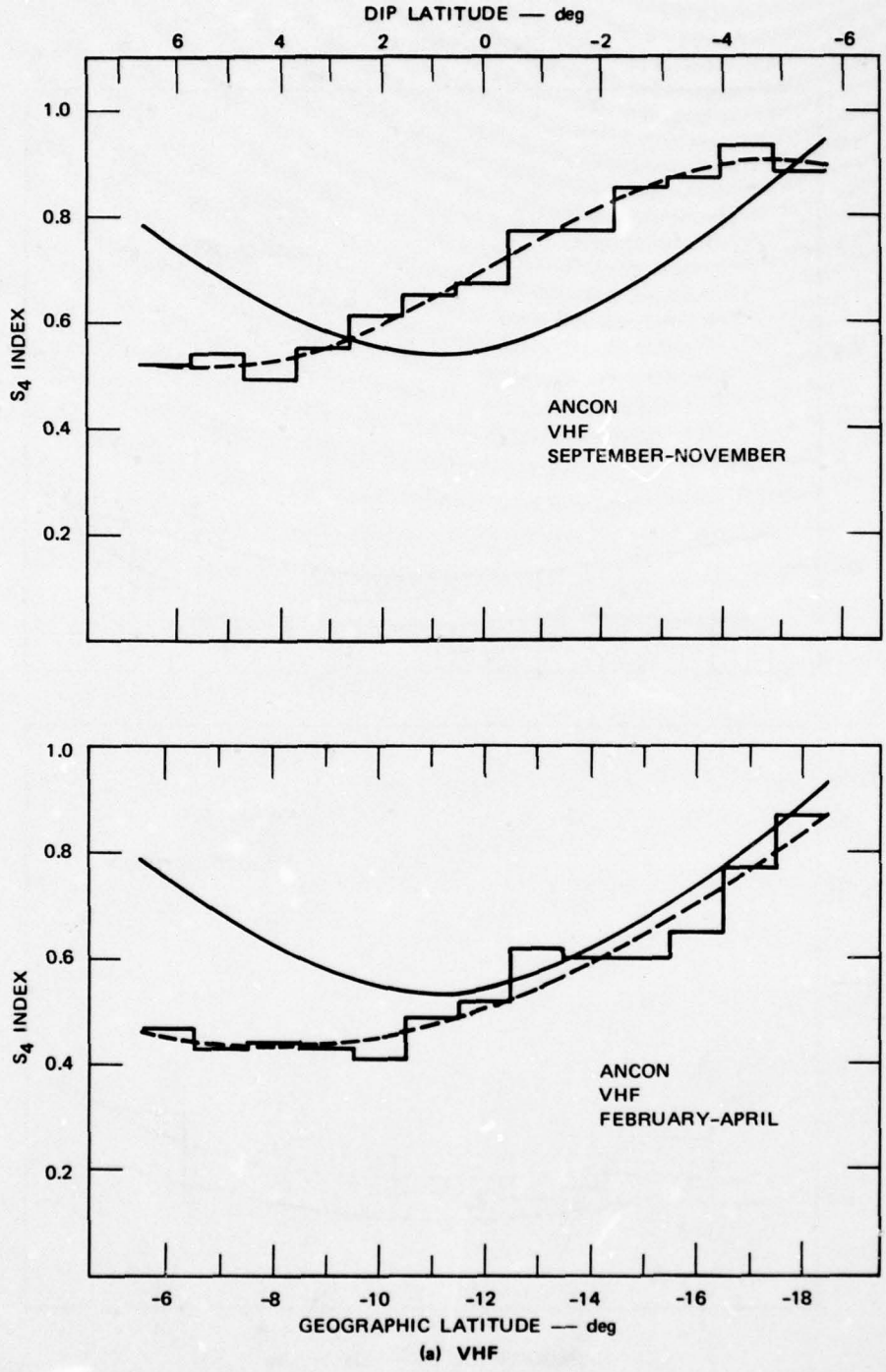


FIGURE 13 LATITUDE DISTRIBUTIONS OF MEASURED AND PREDICTED MEDIAN $S_4$ AT ANCON, SPRING AND FALL PERIODS

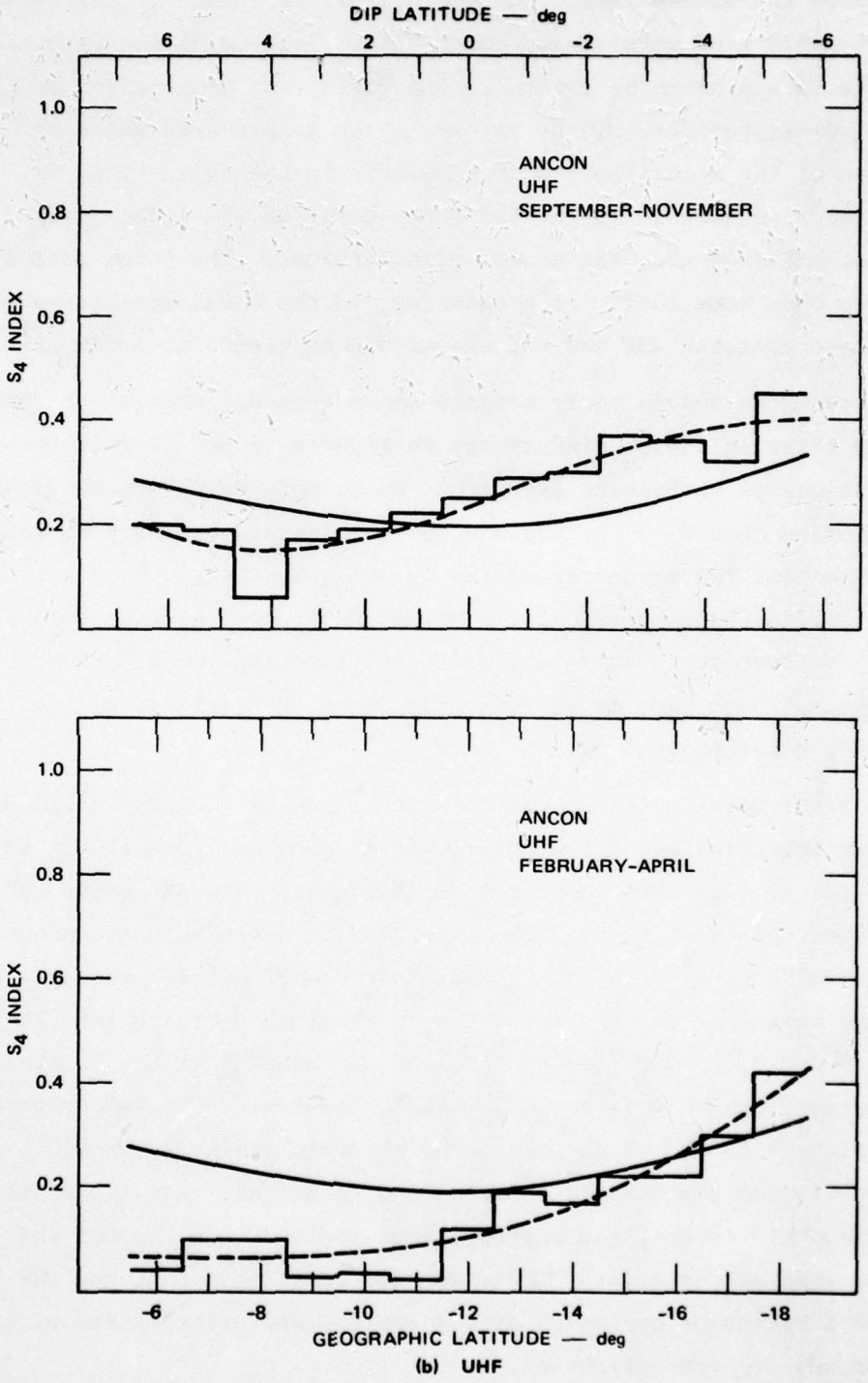


(b) UHF

FIGURE 13 (Concluded)

as shown by the dashed line. The comparisons in Figure 12 indicate that the reasonably good model-measurement fits to the Kwajalein data seen in Figure 10 appear to be a result of a fortuitous combination of changing seasonal distributions. There appears to be a northward shift or extension of the scintillation at Kwajalein in the fall. This is particularly noticeable in the VHF data, although the least-squares fit curves at UHF show the same trends with latitude. The Ancon data in Figure 13 show some shift, or broadening, in the local springtime data. Again, note that the VHF and UHF measured data trends at Ancon are similar.

We can more conveniently compare these seasonal changes at the two sites by relating the $S_4$ differences in Figures 12 and 13 to latitudinal distributions of turbulence strength. We do this using the weak-scatter approximation that $S_4^2 \propto C_s$, where $C_s$ is the in-situ strength of turbulence. By differencing the predicted median $S_4$ and a least-squares fit to the measured median $S_4$ in terms of $C_s$, we obtain Figure 14. The turbulence strength difference is in relative dB, and for each UHF-VHF pair, the distributions have been adjusted to place the VHF-implied value of $C_s$ at the dip equator, at 0 dB.

We first point out that the data in Figure 14 qualify the method we have used to estimate the irregularity distributions from the $S_4$ data. For two out of four three-months sets (Kwajalein Fall and Ancon Spring) we see good agreement between the irregularity distributions calculated from the VHF and UHF data sets. These match well despite the very different nature of the UHF and VHF $S_4$ exceedance distributions in Figures 8 and 9. The difference between UHF and VHF in the remaining two distributions can be attributed to the low median UHF $S_4$ values for these sets. Figures 12 and 13 show that the observed median $S_4$ drops to near noise levels for the Kwajalein spring and Ancon fall data. Despite the distortion this causes, the distributions implied from the UHF and VHF data are generally similar. Thus, we have confidence that the VHF results are good first-order estimates of the latitudinal distribution of scintillation-producing irregularities.

The Ancon and Kwajalein data are plotted in Figure 14 with dip latitudes aligned to emphasize two points. First, the regions of enhanced

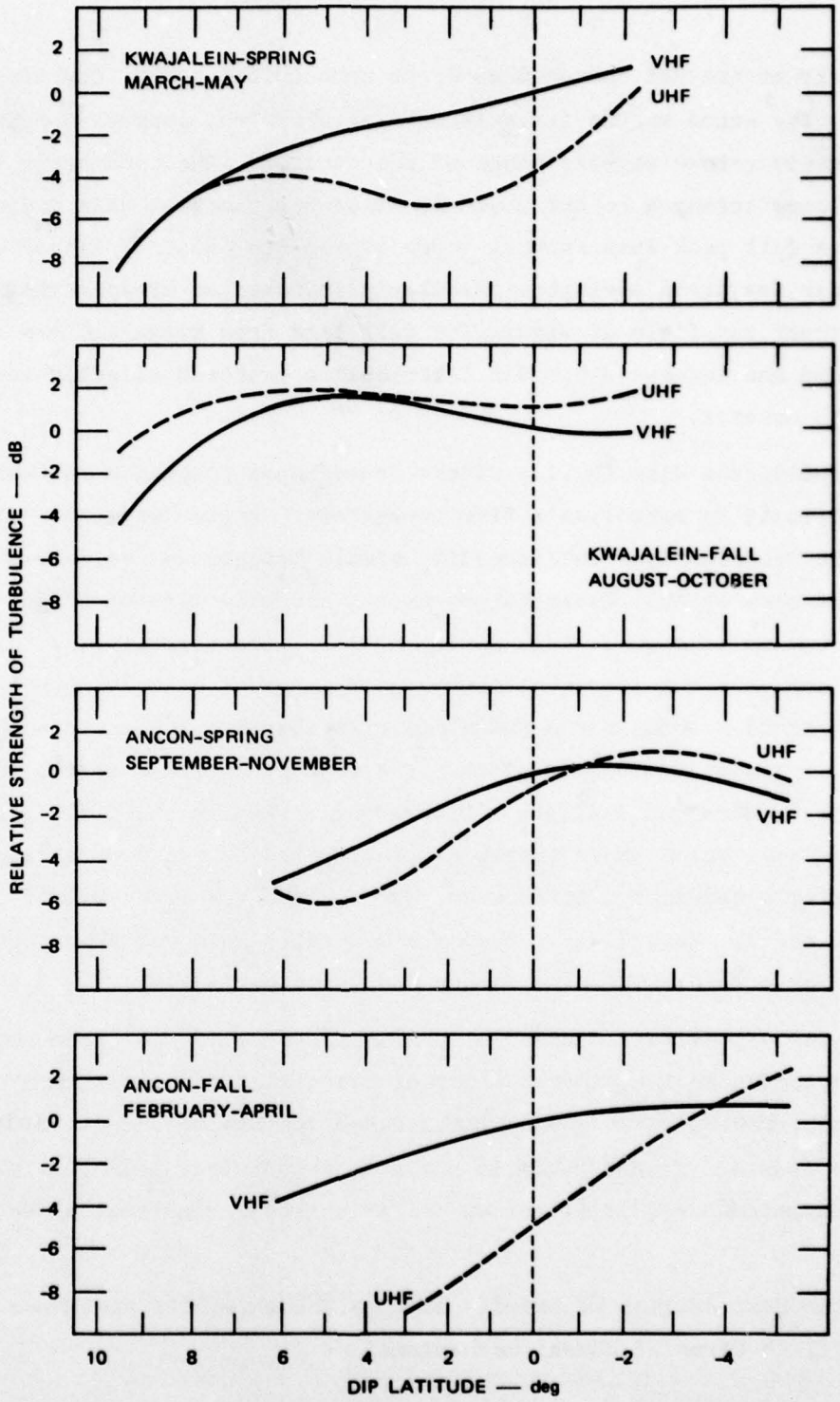


FIGURE 14 LATITUDE DISTRIBUTIONS OF RELATIVE TURBULENCE STRENGTH DERIVED FROM $S_4$ MEASUREMENT-MODEL COMPARISONS AT KWAJALEIN AND ANCON, SPRING AND FALL PERIODS. Both UHF and VHF derived distributions are shown.

irregularities are not centered upon, or symmetrical about, the dip equator. The Ancon spring irregularity perturbations appear to peak approximately 2-to-4 degrees south of the equator. The consistent increase in turbulence strength to the south of Ancon for the fall data would indicate a fall peak even further south of the dip equator. The distributions for Kwajalein springtime similarly indicate an irregularity peak well south of our field of view. The fall data from Kwajalein are more complicated and suggest a binodal distribution centered slightly south of the dip equator.

Secondly, the distribution widths depend upon longitude and season. It is difficult to establish a firm irregularity region width for all but one of the distributions in Figure 14, simply because we see only a portion of the region. Nevertheless we can estimate minimum widths and observe seasonal changes. From spring to fall, the irregularity turbulence band at Ancon (3-dB half-width) increases from about 5° to something greater than 8°. Both of the Kwajalein distributions appear to be much broader, at least 10° in half-width. The rate of increase to the south in the spring data may indicate a broader band than in the fall. These widths are well below those that would be implied by eye from a single, weak-scatter exceedance distribution, such as the VHF $S_4 > 0.2$ of Figures 8 and 9. Accordingly, they are generally narrower than those found in the previous VHF experiments mentioned earlier.

Figure 14 provides statistically significant evidence, from two observation frequencies, that equatorial scintillation arises from enhanced irregularity regions that change with season and are not necessarily dip-equator centered. Perhaps this is one reason that Taur (1974) at gigahertz frequencies sees little order in his worldwide latitudinal dependence data.

In the next section we briefly discuss these results and those from Section III in terms of causal mechanisms.

# V DISCUSSION

In terms of systems applications, the results in this report are straightforward. Using the Wideband beacon we have measured the severity of nighttime signal intensity scintillation at two locations near the equator, as a function of season, frequency, latitude, and propagation geometry. The data are presented in terms of the cumulative distributions of $S_4$ index at VHF, UHF, and L-band frequencies. The $S_4$ index provides a precise measure of the scintillation level, which, as we have demonstrated, can be readily and accurately converted to the distribution of signal intensity. Thus, Figures 3 and 4 can be used to obtain, for example, fade depth distributions occurring a given percentage of the time, as a function of season, at the equator. The consistent frequency dependence of $S_4$ at each station means that our data can be accurately extrapolated to frequencies of interest ranging from probably 50 MHz to a few gigahertz.

These same comments apply to the latitudinal distributions of $S_4$ given in Figures 8 and 9. Here, however, the severity of scintillation is modified by changes in propagation geometry. Our data are directly applicable to moving satellites with moderate to high orbital inclinations. For applications to geostationary beacons, the geometrical factors should be removed. The comparisons of Section IV show that these geometrical effects are accurately described by a simple phase screen model with elongated, field-aligned irregularities.

The other aspect of our scintillation morphology results concerns the physics of irregularity generation. This includes the observed northern/southern hemisphere local summer centering of the scintillation season, the short and medium-term systematic variabilities in the occurrence of scintillation, and the concentration of irregularities away from the dip equator. We suggest that these results indicate that neutral atmosphere perturbations play a major role in the generation of scintillation-producing irregularities.

One strong, albeit indirect, argument for a neutral-atmosphere influence on equatorial scintillation is that the 8-to-9-month active season is centered around local summer. This is clearly the case with our Kwajalein and Ancon data. Local summer is a geographic definition; now consider that Ancon is within a fraction of a degree of the dip equator. If the scintillation is primarily associated with an instability mechanism that acts over extended regions of flux tubes (as, for example, the Rayleigh-Taylor instability should) would we still expect to see this same geographic dominance and seasonal behavior?

Perturbations in the equatorial ionosphere attributed to acoustic gravity waves have been observed, or implied, for some time. This includes incoherent-scatter studies (Sterling et al., 1971), and HF studies (Rottger, 1977) of medium-scale TIDs. Quasi-periodic structures, typically a few percent of the observed total content, are also a consistent feature in the Wideband data.

Of interest to us here is the observed association between one edge of these wave-like structures and regions of enhanced scintillation. This phenomenon is currently under study and will be discussed in a future report. It will suffice to say here that the association is consistent up through moderate scattering conditions at UHF; with more severe scintillation the large-scale structures become distorted and the correlation with scintillation becomes more difficult. These severe scattering conditions are almost surely associated with the plumes, as predicted by the Rayleigh-Taylor modeling, and constitute some small portion of the scintillation we observe (see Figures 3 and 4). We suggest that the bulk of our scintillation data, which is only weak to moderate in severity, arises not from the Rayleigh-Taylor instability, but from the nonlinear steepening of medium-scale TIDs. Whether these waves are amplified by spatial resonance, as suggested by Rottger (1978), or simply by propagation under fortuitous conditions, is not clear.

Irregularity generation due to neutral-wave/ionosphere interaction is generally consistent with the other features we have noted in this report. Medium-scale TIDs observed away from the equator (Munro, 1958)

change direction with season. If this is also true at the equator, only regions with a certain range of magnetic declination should be susceptible to spatial-resonance TID growth. This is because spatial-resonance growth depends, among other factors, upon the wave direction with respect to the local magnetic field. This could account for the seasonally dependent, non-dip-equator-aligned regions of irregularities that we observe, and conceivably for the overall seasonal dependence of scintillation that we observe. Similarly, the short -and medium-term variabilities we observe in scintillation occurrence might also be explained by changes in the direction or speed of neutral atmosphere waves.

Although these effects dominate our statistics, we also see indications of more than one irregularity mechanism at work in the equatorial ionosphere. Our evidence is that the seasonal changes in $S_4$ exceedance do not always track from VHF to UHF to L-band. This is not to say, as pointed out in Section III, that the $S_4$ exceedance levels at two frequencies for a given turbulence strength (e.g., $\sim S_4 > 0.8$ at VHF and $\sim S_4 > 0.2$ at UHF) do not track. In fact these track well over the limited $S_4$ range that we can compare from one frequency to the next. On the other hand, if we consider the same weak-scatter ($S_4 > 0.2$ or $S_4 > 0.4$) levels at VHF versus L-band, we are dealing with turbulence strength differences of roughly 30 dB. As we have suggested above, at VHF we are probably dealing with neutral-wave perturbation-generated irregularities; at L-band the orders-of-magnitude-stronger, yet less prevalent, irregularities are probably a product of the Rayleigh-Taylor instability. It is not too surprising, then, to see periods in Figures 3 and 4 during which the seasonal trends do not track from VHF through L-band. At both sites these

periods are during the spring and fall. These may be times during which the ionosphere is in change and is becoming less susceptible to neutral-wave perturbations and more susceptible to the plumes. Accordingly, the $S_4$ occurrence at VHF may drop while that at L-band increases, or vice versa. Despite this partial independence of the two mechanisms, they still remain closely tied, as we can see by the overall seasonal behavior at VHF, UHF, and L-band. The "geographic" dependence of the scintillation season may, in turn, imply that the neutral-wave perturbations act as a trigger in plume generation.

## REFERENCES


Aarons, J., "Equatorial Scintillations: A Review," AFGL-TR-76-0078, Air Force Geophysics Laboratory, Hanscom AFB, MA (1976).

Basu, S., S. Basu, and B. H. Khan, "Model of Equatorial Scintillations from In-Situ Measurements," Radio Sci., Vol. 11, p. 821 (1976).

Briggs, B. H. and I. A. Parkin, "On the Variation of Radio Star and Satellite Scintillation with Zenith Angle," J. Atmos. Terr. Phys., Vol. 25, p. 339 (1963).

Calvert W. and C. W. Schmid, "Spread-F Observations by the Alouette Topside Sounder Satellite," J. Geophys. Res., Vol. 69, p. 1893 (1964).

Chatterjee, S. K., A. K. Bandyopadhyay, B. K. Guhathakurla, and P. Bandyopadhyay, "The Equatorial Scintillation Belt as Observed at Huancayo, Peru," Am. Geophys., Vol. 30, No. 2, p. 329 (1974).

Fremouw, E. J., C. L. Rino, A. R. Hessing, and V. E. Hatfield, "A Transionospheric Communication Channel Model," Quarterly Technical Report 7, Contract F30602-75-C-0236, SRI Project 4259, Stanford Research Institute, Menlo Park, CA (1977).

Fremouw, E. J., R. L. Leadabrand, R. C. Livingston, M. D. Cousins, C. L. Rino, B. C. Fair, and R. A. Long, "Early Results from the DNA Wideband Satellite Experiment--Complex-Signal Scintillation," Radio Sci., Vol. 13, No. 1, p. 167 (1978).

Golden, T. S., "Ionospheric Distortion of Mini Track Signals in South America," GSFC Report X-525-68-56, Goddard Space Flight Center, Greenbelt, MD (1968).

IAGA Commission 2 Working Group 4, "International Geomagnetic Reference Field 1965.0," J. Geophys. Res., Vol. 74, p. 4407 (1969).

Kelley, M. C., G. Haerendel, H. Kappler, A. Valenzuela, B. B. Balsley, D. A. Carter, W. L. Ecklund, C. W. Carlson, B. Hansler, and R. Torbert, "Evidence for a Rayleigh-Taylor Type Instability and Upwelling of Depleted Density Regions During Equatorial Spread-F," Geophys. Res. Letts., Vol. 3, p. 448 (1976).

Koster, J. R., "Equatorial Scintillation," Planet. Space Sci., Vol. 20, p. 1999 (1972).

Koster, J. R., "Equatorial Studies of the VHF Signal Radiated by Intelsat II, F-3. Ionospheric Scintillation," University of Ghana, Accra, Ghana, AD 681462 (1968).

McClure, J. P., W. B. Hanson, and J. H. Hoffman, "Plasma Bubbles and Irregularities in the Equatorial Ionosphere," J. Geophys. Res., Vol. 82, p. 2650 (1977).

Morse, F. A., B. C. Edgar, H. C. Koons, C. J. Rice, W. J. Heikkila, J. H. Hoffman, B. A. Tinsley, J. D. Winningham, A. B. Christensen, R. G. Woodman, J. Pomalaza, and N. R. Teixeira, "Equion, An Equatorial Ionospheric Irregularity Experiment," J. Geophys. Res., Vol. 82, p. 578 (1977).

Munro, G. H., "Travelling Ionospheric Disturbances in the F-Region," Aust. J. Phys., Vol. 11, p. 91 (1958).

Nichols, B. E., Technical Note of Lincoln Laboratory, 1974-19, Massachusetts Institute of Technology, Lexington, MA (1974).

Paulson, M. R. and R. U. F. Hopkins, "Effects of Equatorial Scintillation Fading on Satcom Signals," NELC Report TR 1875, Naval Electronics Laboratory Center, San Diego, CA (1973).

Rino, C. L. and R. C. Livingston, "A Spaced-Receiver Data Analysis Technique for Simultaneously Estimating Anisotropy and Pattern Drifts in Radio Wave Transmission Experiments," Topical Report 4, Contract DNA001-77-C-0220, SRI Project 6434, SRI International, Menlo Park, CA (in preparation, 1978).

Rino, C. L. and S. J. Matthews, "On the Interpretation of Ionospheric Scintillation Data Using a Power-Law Phase-Screen Model--Weak Scatter," DNA 4606T, Topical Report 2, Contract DNA001-77-C-0220, SRI Project 6434, SRI International, Menlo Park, CA (1978).

Rottger, J., "Drifting Patches of Equatorial Spread-F Irregularities--An Experimental Support for the Spatial Resonance Mechanism in the Ionosphere," preprint (1978).

Rottger, J., "Travelling Disturbances in the Equatorial Ionosphere and their Association with Penetrative Cumulus Convection," J. Atmos. Terr. Phys., Vol. 39, p. 987 (1977).

Scannapieco, A. J. and S. L. Ossakow, "Nonlinear Equatorial Spread-F," Geophys. Res. Letts., Vol. 3, p. 341 (1976).

Sinclair, J. and R. F. Kelleher, "The F-Region Equatorial Irregularity Belt as Observed from Scintillation of Satellite Transmissions," J. Atmos. Terr. Phys., Vol. 31, p. 201 (1969).

Sterling, D. L., W. H. Hooke, and R. Cohen, "Traveling Ionospheric Disturbances Observed at the Magnetic Equator," J. Geophys. Res., Vol. 76, p. 3777 (1971).

Taur, R. R., "Ionospheric Scintillation at 4 and 6 GHz," ComSat Tech. Rev., Vol. 3, p. 145 (1973).

Tsunoda, R. T., M. J. Baron, and J. Owen, "ALTAIR: An Incoherent Scatter Radar for Equatorial Spread-F Studies," DNA 4538T, Topical Report 1, Contract DNA001-77-C-0220, SRI Project 6434, SRI International, Menlo Park, CA (1978).

Whitney, H. E., "Notes on the Relationship of Scintillation Index to Probability Distributions and Their Uses for System Design," AFGRL Report TR-75-0004, Air Force Geophysics Laboratory, Hanscom AFB, MA (1974).

Woodman, R. F. and C. La Hoz, "Radar Observations of F Region Equatorial Irregularities," J. Geophys. Res., Vol. 81, p. 5447 (1976).

Wright, R. W. H., "Geomorphology of Spread-F and Characteristics of Equatorial Spread-F," J. Atmos. Terr. Phys., Vol. 64, p. 2203 (1959).

# DISTRIBUTION LIST

DEPARTMENT OF DEFENSE

Assistant Secretary of Defense
Comm, Cmd, Cont. & Intell.
ATTN: M. Epstein
ATTN: J. Babcock

Assistant to the Secretary of Defense
Atomic Energy
ATTN: Executive Assistant

Command & Control Technical Center
Department of Defense
ATTN: C-312, R. Mason
ATTN: C-650, G. Jones
ATTN: C-650, W. Heidig

Defense Advanced Rsch. Proj. Agency
ATTN: TIO

Defense Communication Engineer Center
ATTN: Code 720, J. Worhtington
ATTN: Code R410, J. McLean

Defense Communications Agency
ATTN: Code 810, J. Barna
ATTN: Code 480
ATTN: Code 101B
ATTN: Code R1033, M. Raffensperger

Defense Documentation Center
12 cy ATTN: DD

Defense Intelligence Agency
ATTN: DC-7D, W. Wittig
ATTN: DB-4C, E. O'Farrell
ATTN: HQ-TR, J. Stewart
ATTN: DB, A. Wise
ATTN: DT-5
ATTN: DT-1BZ, R. Morton
ATTN: DT-1B

Defense Nuclear Agency
ATTN: DDST
ATTN: STVL
3 cy ATTN: RAAE
4 cy ATTN: TITL

Field Command,
Defense Nuclear Agency
ATTN: FCPR

Interservice Nuclear Weapons School
ATTN: TTV

Joint Chiefs of Staff
ATTN: J-3, WWMCCS Evaluation Office

Joint Strat. Tgt. Planning Staff
ATTN: JPST, G. Goetz
ATTN: JLTW-2

Livermore Division, Field Command, DNA
Lawrence Livermore Laboratory
ATTN: FCPRL

DEPARTMENT OF DEFENSE (Continued)

National Security Agency
Department of Defense
ATTN: R52, J. Skillman
ATTN: B3, F. Leonard
ATTN: W32, O. Bartlett

Under Secretary of Defense for Rsch. & Engrg.
ATTN: Strategic & Space Systems (OS)

WWMCCS System Engineering Org.
ATTN: R. Crawford

DEPARTMENT OF THE ARMY

Atmospheric Sciences Laboratory
U.S. Army Research & Development Command
ATTN: DELAS-AE-M, F. Niles

ERADCOM Technical Support Activity
Department of the Army
ATTN: DELET-ER, H. Bomke

Harry Diamond Laboratories
Department of the Army
ATTN: DELHD-N-NP
ATTN: DELHD-N-RB, R. Williams
ATTN: DELHD-N-NP, F. Wimenitz
ATTN: DELHD-N-TI, M. Weiner

U. S. Army Comm-Elec. Engrg. Instal. Agency
ATTN: CCC-EMEO, W. Nair
ATTN: CCC-EMEO, PED, G. Lane

U.S. Army Foreign Science & Tech. Center
ATTN: DRXST-SD

U.S. Army Materiel Dev. & Readiness Command
ATTN: DRCLDC, J. Bender

U.S. Army Nuclear & Chemical Agency
ATTN: Library

U.S. Army Satellite Comm. Agency
ATTN: Document Control

DEPARTMENT OF THE NAVY

Naval Electronic Systems Command
ATTN: NAVELEX 3101, T. Hughes
ATTN: PME 117
ATTN: Code 5011
ATTN: PME 117-T

Naval Intelligence Support Center
ATTN: NISC-50

Naval Ocean Systems Center
ATTN: Code 0230, C. Baggett
3 cy ATTN: Code 532, W. Moler

Naval Space Surveillance System
ATTN: J. Burton

DEPARTMENT OF THE NAVY (Continued)

Naval Research Laboratory
ATTN: Code 6700, T. Coffey
ATTN: Code 6707, J. Davis
ATTN: Code 6701, J. Brown
ATTN: Code 7580
ATTN: Code 7555
ATTN: Code 7500, Hg. Comm. Dir., B. Wald

Naval Surface Weapons Center
ATTN: Code F31

Naval Surface Weapons Center
Dahlgren Laboratory
ATTN: Code F-14, R. Butler

Office of Naval Research
ATTN: Code 420
ATTN: Code 421

Office of the Chief of Naval Operations
ATTN: Op-604
ATTN: Op-941

Strategic Systems Project Office
Department of the Navy
ATTN: NSSP-2722, F. Wimberly
ATTN: NSP-2141

DEPARTMENT OF THE AIR FORCE

Aerospace Defense Command/DC
Department of the Air Force
ATTN: DC, Mr. Long

Aerospace Defense Command/XPD
Department of the Air Force
ATTN: XPDQ
ATTN: XP

Air Force Avionics Laboratory
ATTN: AAD, W. Hunt
ATTN: AAD, A. Johnson

Air Force Geophysics Laboratory
ATTN: LKB, K. Champion
ATTN: OPR1, J. Ulwick
ATTN: PHP, J. Aarons
ATTN: PHI, J. Buchau
ATTN: PHP, J. Mullen
ATTN: OPR, A. Stair

Air Force Weapons Laboratory
ATTN: DYC, J. Barry
ATTN: SUL
ATTN: DYC, J. Kamm

Deputy Chief of Staff
Research, Development, & Acq.
Department of the Air Force
ATTN: AFRDQ

Deputy Chief of Staff
Program and Analyses
Department of the Air Force
ATTN: PACSC, R. Paul

DEPARTMENT OF THE AIR FORCE (Continued)

Electronic Systems Division, AFSC
ATTN: DCKC, J. Clark
ATTN: XRW, J. Deas
ATTN: YSEA

Foreign Technology Division, AFSC
ATTN: TQTD, B. Ballard
ATTN: NIIS, Library

Ogden ALC/MMEDDE
Department of the Air Force
ATTN: OO-ALC/MM, R. Blackburn

Rome Air Development Center, AFSC
ATTN: V. Coyne, OCSE
ATTN: Documents Library/TSLD

Rome Air Development Center, AFSC
ATTN: EEP

Space & Missile Systems Organization/SK
Air Force Systems Command
ATTN: SKA, M. Clavin

Strategic Air Command/XPFS
Department of the Air Force
ATTN: NRT
ATTN: DCX, Chief Scientist

DEPARTMENT OF ENERGY

Department of Energy
Albuquerque Operations Office
ATTN: Doc. Con. for D. Sherwood

Department of Energy
Library Room G-042
ATTN: Doc. Con. for A. Labowitz

Office of Military Application
Department of Energy
ATTN: Doc. Con. for D. Gale

OTHER GOVERNMENT AGENCIES

Central Intelligence Agency
ATTN: RD/SI, Rm. 5G48, Hq. Bldg.
for OSI/PSTD

Department of Commerce
National Bureau of Standards
ATTN: Sec. Officer for R. Moore

Department of Transportation
Office of the Secretary
ATTN: R. Lewis
ATTN: R. Doherty

Institute for Telecommunications Sciences
National Telecommunications & Info. Admin.
ATTN: L. Berry
ATTN: A. Jean
ATTN: W. Utlaut
ATTN: D. Crombie

OTHER GOVERNMENT AGENCIES (Continued)

National Oceanic & Atmospheric Admin.
Environmental Research Laboratories
Department of Commerce
ATTN: Aeronomy Lab., G. Reid
ATTN: R. Grubb

DEPARTMENT OF DEFENSE CONTRACTORS

Aerospace Corp.
ATTN: F. Morse
ATTN: N. Stockwell
ATTN: I. Garfunkel
ATTN: D. Olsen
ATTN: S. Bower
ATTN: J. Carter
ATTN: T. Salmi
ATTN: V. Josephson
ATTN: R. Slaughter

Analytical Systems Engineering Corp.
ATTN: Radio Sciences

Berkeley Research Associates, Inc.
ATTN: J. Workman

Boeing Co.
ATTN: J. Kenney
ATTN: G. Keister
ATTN: D. Murray
ATTN: G. Hall
ATTN: S. Tashird

Brown Engineering Company, Inc.
ATTN: R. Deliberis

University of California at San Diego
ATTN: H. Booker

Charles Stark Draper Lab., Inc.
ATTN: D. Cox
ATTN: J. Gilmore

Computer Sciences Corp.
ATTN: H. Blank

Comsat Labs.
ATTN: G. Hyde
ATTN: R. Taur

Cornell University
Department of Electrical Engineering
ATTN: D. Farley, Jr.

Electrospace Systems, Inc.
ATTN: H. Logston

ESL, Inc.
ATTN: C. Prettie
ATTN: J. Roberts
ATTN: J. Marshall

Ford Aerospace & Communications Corp.
ATTN: J. Mattingley

General Electric Co.
Space Division
ATTN: M. Bortner, Space Sci. Lab.

General Electric Co.
ATTN: F. Reibert

DEPARTMENT OF DEFENSE CONTRACTORS (Continued)

General Electric Company-TEMPO
Center for Advanced Studies
ATTN: W. Knapp
ATTN: M. Stanton
ATTN: B. Gambill
ATTN: T. Stevens
ATTN: D. Chandler
ATTN: DASIAC

General Electric Tech. Services Co., Inc.
HMES
ATTN: G. Millman

General Research Corp.
Santa Barbara Division
ATTN: J. Ise, Jr.
ATTN: J. Garbarino

Geophysical Institute
University of Alaska
ATTN: Sec. Office for N. Brown
ATTN: Sec. Office for T. Davis
ATTN: Sec. Office for Technical Library

GTE Sylvania, Inc.
Electronics Systems Grp.-Eastern Div.
ATTN: M. Cross

HSS, Inc.
ATTN: D. Hansen

University of Illinois
ATTN: Sec. Supervisor for K. Yeh

Institute for Defense Analyses
ATTN: E. Bauer
ATTN: J. Aein
ATTN: J. Bengston
ATTN: H. Wolfhard

International Tel. & Telegraph Corp.
ATTN: Technical Library

JAYCOR
ATTN: S. Goldman

Johns Hopkins University
Applied Physics Lab.
ATTN: T. Potemra
ATTN: Document Librarian
ATTN: T. Evans

Kaman Sciences Corp.
ATTN: T. Meagher

Lawrence Livermore Laboratory
University of California
ATTN: Doc. Con. for Technical Information
Dept. Library
ATTN: Doc. Con. for L-46, F. Seward

Linkabit Corp.
ATTN: I. Jacobs

Lockheed Missiles & Space Co., Inc.
ATTN: Dept. 60-12
ATTN: D. Churchill

DEPARTMENT OF DEFENSE CONTRACTORS (Continued)

Lockheed Missiles and Space Co., Inc.
ATTN: R. Johnson
ATTN: M. Walt, Dept. 52-10
ATTN: W. Imhof, D/52-12

Los Alamos Scientific Laboratory
ATTN: Doc. Con. for D. Westervelt
ATTN: Doc. Con. for R. Taschek
ATTN: P. Keaton

M.I.T. Lincoln Lab.
ATTN: D. Towle
ATTN: L. Loughlin
ATTN: D. Clark
ATTN: P. Waldron

McDonnell Douglas Corp.
ATTN: N. Harris
ATTN: G. Mroz
ATTN: J. Moule
ATTN: W. Olson

Mission Research Corp.
ATTN: R. Hendrick
ATTN: S. Gutsche
ATTN: F. Fajen
ATTN: D. Sowle
ATTN: R. Bogusch
ATTN: M. Scheibe
ATTN: R. Scott
ATTN: D. Knepp

Mitre Corp.
ATTN: C. Callahan
ATTN: G. Harding

Mitre Corp.
ATTN: W. Foster
ATTN: M. Horrocks
ATTN: W. Hall

Pacific-Sierra Research Corp.
ATTN: E. Field, Jr.

Pennsylvania State University
Ionosphere Research Lab.
ATTN: Ionospheric Research Lab.

Photometrics, Inc.
ATTN: I. Kofsky

Physical Dynamics, Inc.
ATTN: E. Fremouw

R & D Associates
ATTN: R. Lelevier
ATTN: B. Gabbard
ATTN: R. Turco
ATTN: F. Gilmore
ATTN: H. Ory
ATTN: W. Karzas
ATTN: W. Wright, Jr.
ATTN: C. MacDonald

DEPARTMENT OF DEFENSE CONTRACTORS (Continued)

Rand Corp.
ATTN: E. Bedrozian
ATTN: C. Crain

Riverside Research Institute
ATTN: V. Trapani

Sandia Laboratories
Livermore Laboratory
ATTN: Doc. Con. for T. Cook
ATTN: Doc. Con. for B. Murphey

Sandia Laboratories
ATTN: Doc. Con. for 3141
ATTN: Doc. Con. for Space Project Div.
ATTN: Doc. Con. for D. Thornbrough
ATTN: Doc. Con. for W. Brown
ATTN: Doc. Con. for D. Dahlgren

Science Applications, Inc.
ATTN: L. Linson
ATTN: D. Hamlin
ATTN: D. Sachs

Science Applications, Inc.
Huntsville Division
ATTN: D. Divis

Science Applications, Inc.
ATTN: SZ

SRI International
ATTN: G. Carpenter
ATTN: R. Livingston
ATTN: C. Rino
ATTN: G. Smith
ATTN: G. Price
ATTN: R. Leadabrand
ATTN: W. Jaye
ATTN: W. Chesnut
ATTN: M. Baron
ATTN: A. Burns
ATTN: D. Neilson

Tri-Com, Inc.
ATTN: D. Murray

TRW Defense & Space Sys. Group
ATTN: S. Altschuler
ATTN: R. Plebuch
ATTN: D. Dee

Visidyne, Inc.
ATTN: J. Carpenter

Utah State University
Contract/Grant Office
Space Science Laboratory
ATTN: K. Baker
ATTN: L. Jensen